DIGRAC: Digraph Clustering with Flow Imbalance

Yixuan He
Department of Statistics
University of Oxford
yixuan.he@stats.ox.ac.uk

Gesine Reinert
Department of Statistics
University of Oxford &
The Alan Turing Institute, London, UK
reinert@stats.ox.ac.uk

Mihai Cucuringu
Department of Statistics and Mathematical Institute
University of Oxford &
The Alan Turing Institute, London, UK
mihai.cucuringu@stats.ox.ac.uk

Abstract

Node clustering is a powerful tool in the analysis of networks. Here, we introduce a graph neural network framework with a novel scalable *Directed Mixed Path Aggregation* (DIMPA) scheme to obtain node embeddings for directed networks in a self-supervised manner, including a novel probabilistic imbalance loss. The method is end-to-end in combining embedding generation and clustering without an intermediate step. In contrast to standard approaches in the literature, in this paper, directionality is not treated as a nuisance, but rather contains the main signal. In particular, we leverage the recently introduced *cut flow imbalance* measure, which is tightly related to directionality; cut flow imbalance is optimized without resorting to spectral methods or cluster labels. Experimental results on synthetic data, in the form of directed stochastic block models and real-world data at different scales, demonstrate that our method attains state-of-the-art results on directed graph clustering, for a wide range of noise and sparsity levels and graph structures.

1 Introduction

Revealing the underlying community structure of *directed* networks (*digraphs*) is an important problem in various application domains [30], such as detecting influential groups in social networks [5]. Node clustering in digraphs can be a successful approach for this community detection task [35]. While most existing works on directed clustering rely on edge densities instead of direction, we argue the latter can play a vital role in directed clustering as it can reveal latent properties of network flows. Therefore, instead of finding relatively dense groups of nodes in digraphs which have a relative small amount of flow between the groups, as in [17, 34, 28, 26, 8, 22], our ,main goal is to recover clusters with strong and imbalanced flow among them, in the spirit of [12, 25], where directionality (i.e, edge orientation) is the main signal. In contrast to standard approaches focusing on edge density, here edge directionality is not a nuisance but the main piece of information to uncover the latent structure. The underlying intuition is that homogeneous clusters of nodes form *meta-nodes* in a *meta-graph*, with the meta-graph directing the flow between clusters; directed core-periphery structure is such an example [15]. Figure 1(a) shows an example of cut imbalance between two clusters, here for an unweighted network for simplicity: while 75% of the edges flow from the *Transient* cluster to the *Sink* cluster, only 25% flow in the other direction. A real-world example of flow imbalance between

Preprint. Under review.

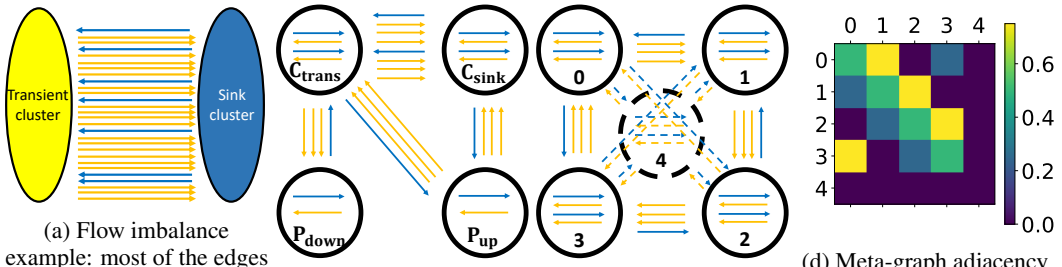

(a) Flow imbalance example: most of the edges flow from *Transient* to *Sink*. (b) Flow on *Telegram* data. (c) Meta-graph. (d) Meta-graph adjacency matrix $\mathbf{F}$.

Figure 1: Visualization of cut flow imbalance and meta-graph: (a) 75% of edges flow from Transient to Sink, while 25% of edges flow in the opposite direction; (b) flow on *Telegram* data [5]: most edges flow from C_{trans} to C_{sink}; (c) & (d) are for a Directed Stochastic Block Model with a cycle meta-graph with ambient nodes, for a total of 5 clusters. 75% of the edges flow in direction $0 \to 1 \to 2 \to 3 \to 0$, while 25% flow in the opposite direction. Cluster 4 is the ambient cluster. In (c), the directions of flow in dashed lines and flow within clusters are random. Flow in dashed lines do not exist in the meta-graph adjacency matrix $\mathbf{F}$. For (d), the lighter the color, the stronger the flow.

four clusters of the (weighted) Telegram Britain First Network [5] is given in Figure 1(b); most edges flow from the core *Transient* cluster (C_{transe}) to the core *Sink* cluster (C_{sink}).

Competitive state-of-the-art methods proposed for node clustering in digraphs are somewhat limited in scope – most of them mainly rely on edge density and overlook the role of directionality [17, 34, 28, 26, 8, 22], and those that lay emphasis on directionality, usually by incorporating cut imbalance among clusters, are mainly based on spectral methods or require labeling information.

In this paper, we introduce a graph neural network (GNN) framework, denoted DIGRAC, with a novel *DIrected Mixed Path Aggregation* (DIMPA) scheme, to obtain node embeddings for clustering digraphs (potentially weighted, possibly with self-loops, but no multiple edges), with an efficient implementation. The use of powers of adjacency matrices, instead of multi-layers as in [24], for the purpose of neighborhood information aggregation, was sparked by a mechanism for node feature aggregation proposed in [41], focused on undirected networks. In a self-supervised manner, a novel *probabilistic imbalance loss* is proposed to act on the digraph induced by all training nodes. The method is end-to-end in combining embedding generation and clustering without an intermediate step. To the best of our knowledge, this is the first GNN-based method that derives node embeddings for digraphs that directly maximizes the cut imbalance between pairs of clusters.

Experimental results on synthetic data and real-world data at different scales –namely, *Telegram* [5], *Blog* [1], *Migration* [36], and *WikiTalk* [27], demonstrate that our method can achieve state-of-the-art performance for a wide range of network densities and topologies. Compared to its competitors, for synthetic data, our method achieves superior performance (with respect to the Adjusted Rand Index (ARI) [21]); for the real-world data, our experimental results indicate that our method outperforms them, using imbalance scores as outcome measures. We also apply our loss function to the tasks of node classification and link direction prediction, and witness a modest average gain in accuracy on the benchmark data sets *Cora-ML* and *CiteSeer* [4].

The applicability and impact of our work extends beyond applications where the input data is a digraph; for example, when considering time series data as input, the digraph construction mechanism can accommodate any procedure that encodes a pairwise directional association between the corresponding time series, such as lead-lag relationships and Granger causality [40] that can facilitate the analysis of information flow in brain networks [14].

As another use case, consider a social network where a set of fake accounts $\mathcal{A}$ have been created which are likely to target another subset $\mathcal{B}$ of real accounts by sending them messages. Most likely, there would be many more messages from $\mathcal{A}$ to $\mathcal{B}$ compared to from $\mathcal{B}$ to $\mathcal{A}$, hinting that $\mathcal{A}$ is most likely comprised of fake accounts. In ranking applications, where the match results (or preference relationships between items) are encoded in a digraph, our algorithm would allow for the detection of subsets of players where the relative strength of players in $\mathcal{A}$ is superior to that of players in $\mathcal{B}$, thus facilitating the extraction of partial rankings [10]. Our proposed methodology for extracting flow-driven clusters in digraphs based on higher-order meta-graphs can facilitate tasks in time series analysis, ranking, and anomaly detection, as it allows one to extrapolate from *local* pairwise (directed) interactions to a *global* structure inference, in the high-dimensional low signal-to-noise ratio regime.

Main contributions. Our main contributions are as follows. • (1) We propose a GNN for self-supervised end-to-end node clustering on digraphs, which are possibly attributed and weighted, explicitly taking into account cut flow imbalance. • (2) We propose a probabilistic version of the global imbalance score aggregated from the pairwise normalized cut imbalances, to serve as a self-supervised loss function. To the best of our knowledge, this is the first method directly maximizing cut flow imbalance for node clustering in digraphs using GNNs. • (3) We extend our method to the semi-supervised setting when label information is available.

Paper outline. The rest of this paper is organized as follows. Section 2 reviews existing work. Section 3 introduces our DIGRAC method. Section 4 validates its strength through extensive experiments at different scales, on synthetic and real data. Section 5 draws conclusions and discusses limitations and future works. In Supplementary Information (SI), Section A expands on variants of our model; Section B discusses implementation details; Sections C & D provide additional results.

Anonymized codes and preprocessed data are available at `https://anonymous.4open.science/r/1b728e97-cc2b-4e6a-98ea-37668813536c`.

2 Related Work

Directed clustering has been explored by spectral and GNN-based methods. [39] constructs directed clustering that hinges on symmetrizations of the adjacency matrix, but is not scalable as it requires large matrix multiplication. [38] proposes a spectral co-clustering algorithm, called DI_SIM, for asymmetry discovery, that relies on in-degree and out-degree. Whenever direction is the sole information, such as in a complete network with lead-lag structure derived from time series,a purely degree-based method cannot detect the clusters. While [44] produces two partitions of the node set, one based on out-degree and one based on in-degree, here we produce a partition that simultaneously takes both directions into account. The recent work in [12] seeks to uncover clusters characterized by a strongly imbalanced flow circulating among them, based on eigenvectors of the Hermitian matrix $(\mathbf{A} - \mathbf{A}^T) \cdot i$, where $\mathbf{A}$ is the (normalized) adjacency matrix and i the imaginary unit. MagNet [45] builds upon [12, 32] and introduces a complex Hermitian matrix that encodes undirected geometric structure in the magnitude of its entries, and directional information in their phase; however, it assumes unweighted graphs without self-loops. [25] uncovers higher-order structural information among clusters in digraphs, while maximizing the imbalance of the edge directions; however, its definition of the flow ratio restricts the underlying meta-graph to a path.

[29] and [35] introduce directed graph Laplacians, but these methods are only applicable to strongly connected digraphs, which is hardly the case in sparse networks arising in applications. [33] utilizes convolution-like anisotropic filters based on local subgraph structures (motifs) for semi-supervised node classification tasks in digraphs Nonetheless, it relies on pre-defined structures and fails to handle complex networks. DGCN [43] uses first and second order proximity, constructs three Laplacians, but the method is space and speed inefficient. DiGCN [42] simplifies DGCN, builds a directed Laplacian based on PageRank, and aggregates information dependent on higher-order proximity.

In addition, [45, 33, 43, 42] all require known labels, which are not generally available for real data. While [39, 38, 12, 35, 25] are not able to take advantage of node attributes or node labels. In contrast, we propose a scalable GNN-based method which maximizes a probabilistic version of the imbalance flow, in a self-supervised manner, and which can naturally analyze attributed weighted digraphs.

3 The DIGRAC Method

3.1 Problem definition

Denote a (possibly weighted) digraph with node attributes as $\mathcal{G} = (\mathcal{V}, \mathcal{E}, w, \mathbf{X}_\mathcal{V})$, with $\mathcal{V}$ the set of nodes, $\mathcal{E}$ the set of directed edges or links, and $w \in [0, \infty)^{|\mathcal{E}|}$ the set of edge weights. $\mathcal{G}$ may have self-loops, but no multiple edges. The number of nodes is $n = |\mathcal{V}|$, and $\mathbf{X}_\mathcal{V} \in \mathbb{R}^{n \times d_{\text{in}}}$ is a matrix whose rows encode the nodes' attributes [1]. Such a network can be represented by the attribute matrix $\mathbf{X}_\mathcal{V}$ and the adjacency matrix $\mathbf{A} = (A_{ij})_{i,j \in \mathcal{V}}$, with $\mathbf{A}_{ij} = 0$ if no edge exists from v_i to v_j; if there is an edge e from v_i to v_j, we set $A_{ij} = w_e$, the edge weight. For a digraph, $\mathbf{A}$ is usually asymmetric.

Digraphs often lend themselves to interpreting weighted directed edges as flows, with a meta-graph on clusters of vertices describing the overall flow directions; see Figure 1 for an illustration. A clustering

[1] If no attributes are available, one could use any feature matrix generated from $\mathbf{A}$, such as stacking the eigenvectors of the Hermitian matrix introduced in [12], to construct the feature matrix.

is a partition of the set of nodes into K disjoint sets (the number of clusters) $\mathcal{V} = \mathcal{C}_0 \cup \mathcal{C}_1 \cup \cdots \cup \mathcal{C}_{K-1}$. Intuitively, nodes within a cluster should be similar to each other with respect to flow directions, while nodes across clusters should be dissimilar. In a self-supervised setting, only the number of clusters K is given. In a semi-supervised setting, for each of the K clusters, a fraction of training nodes are selected as seed nodes, for which the cluster membership labels are known before training. The set of seed nodes is denoted as $\mathcal{V}^{\text{seed}} \subseteq \mathcal{V}^{\text{train}} \subset \mathcal{V}$, where $\mathcal{V}^{\text{train}}$ is the set of all training nodes.

For an attributed digraph $\mathcal{G} = (\mathcal{V}, \mathcal{E}, w, \mathbf{X}_{\mathcal{V}})$, a node embedding represents each node $v \in \mathcal{V}$ by a low-dimensional vector $z_v \in \mathbb{R}^{d'}$. When accounting for edge weights and node attributes, this embedding results from a learned transformation function $f(\mathbf{A}, \mathbf{X}_{\mathcal{V}}) \to \mathbf{Z}$, with $\mathbf{Z} \in \mathbb{R}^{n \times d'}$ a d'-dimensional representation of the nodes, and f a learned transformation function, such as a Graph Neural Network (GNN). The goal of semi-supervised clustering is to use the embedding to assign each node $v \in \mathcal{V}$ to a cluster containing some known seed nodes, without knowledge of the underlying flow meta-graph. The corresponding self-supervised clustering task does not use seed nodes.

3.2 Directed Mixed Path Aggregation (DIMPA)

Inspired by [41], in order to build node embeddings, we capture local network information by taking a weighted average of information from neighbors within h hops, instead of using multiple layers as in GCN [24]. To this end, we row-normalize the adjacency matrix, $\mathbf{A}$, to obtain $\overline{\mathbf{A}}^s$. Similar to the regularization discussed in [24], we add a weighted self-loop to each node and normalize by setting $\overline{\mathbf{A}}^s = (\tilde{\mathbf{D}}^s)^{-1}\tilde{\mathbf{A}}^s$, where $\tilde{\mathbf{A}}^s = \mathbf{A} + \tau\mathbf{I}$, and the diagonal matrix $\tilde{\mathbf{D}}^s(i,i) = \sum_j \tilde{\mathbf{A}}^s(i,j)$, for a small value τ, such as 0.5.

The h-hop **source** matrix is given by $(\overline{\mathbf{A}}^s)^h$. We denote the set of *up-to-h-hop* source neighborhood matrices as $\mathcal{A}^{s,h} = \{\mathbf{I}, \overline{\mathbf{A}}^s, \ldots, (\overline{\mathbf{A}}^s)^h\}$. Similarly, for aggregating information when each node is construed as a **target** node of a link, we carry out the same procedure for $\mathbf{A}^T$. We denote the set of up-to-h-hop target neighborhood matrices as $\mathcal{A}^{t,h} = \{\mathbf{I}, \overline{\mathbf{A}}^t, \ldots, (\overline{\mathbf{A}}^t)^h\}$, where $\overline{\mathbf{A}}^t$ is the row-normalized target adjacency matrix calculated from $\mathbf{A}^T$.

Next, we define two feature mapping functions for source and target embeddings, respectively. Assume that for each node in $\mathcal{V}$, a vector of features is available, and summarize these features in the input feature matrix $\mathbf{X}_{\mathcal{V}}$. The source embedding (the superscript s stands for source) is given by

$$\mathbf{Z}^s_{\mathcal{V}} = \left(\sum_{\mathbf{M} \in \mathcal{A}^{s,h}} \omega^s_{\mathbf{M}} \cdot \mathbf{M} \right) \cdot \mathbf{H}^s_{\mathcal{V}} \in \mathbb{R}^{n \times d}, \tag{1}$$

where for each $\mathbf{M}$, $\omega^s_{\mathbf{M}}$ is a learnable scalar, d is the dimension of this embedding, and $\mathbf{H}^s_{\mathcal{V}} = \mathbf{MLP}^{(s,l)}(\mathbf{X}_{\mathcal{V}})$. Here, the hyperparameter l controls the number of layers in the multilayer perceptron (MLP) with ReLU activation; we fix $l = 2$ throughout. Each layer of the MLP has the same number d of hidden units. The target embedding $\mathbf{Z}^t_{\mathcal{V}}$ is defined similarly, with s replaced by t in Eq. (1). Different parameters for the MLPs for different embeddings are possible. After these two decoupled aggregations, we concatenate the embeddings to obtain the final node embedding as a $n \times (2d)$ matrix $\mathbf{Z}_{\mathcal{V}} = \text{CONCAT}\left(\mathbf{Z}^s_{\mathcal{V}}, \mathbf{Z}^t_{\mathcal{V}}\right)$. The embedding vector $\mathbf{z}_i$ for a node v_i is the i^{th} row of $\mathbf{Z}_{\mathcal{V}}$, $\mathbf{z}_i := (\mathbf{Z}_{\mathcal{V}})_{(i,:)} \in \mathbb{R}^{2d}$. An efficient implementation of DIMPA is shown in Algorithm 1; we omit the subscript $\mathcal{V}$ for ease of notation. A complexity analysis of the algorithm is given in SI B.8.

After obtaining the embedding matrix $\mathbf{Z}_{\mathcal{V}}$, we apply a linear layer (an affine transformation) to $\mathbf{Z}_{\mathcal{V}}$, so that the resulting matrix has K columns. Next, we apply the unit *softmax* function to map each row to a probability vector $\mathbf{p}_i \in \mathbb{R}^K$ of length equal to the number of clusters, with entries denoting the probabilities of each node to belong to each cluster. The resulting assignment probability matrix is denoted as $\mathbf{P} \in \mathbb{R}^{n \times K}$. Figure 2 gives an overview of our framework.

3.3 Self-supervised loss for clustering

Our self-supervised loss function is inspired by [12], aiming to cluster the nodes by maximizing a normalized form of cut imbalance across clusters. Before introducing the loss function, we first define probabilistic versions of cuts, imbalance flows, and probabilistic volumes.

• The **probabilistic cut** from cluster $\mathcal{C}_k$ to $\mathcal{C}_l$ is defined as

$$W(\mathcal{C}_k, \mathcal{C}_l) = \sum_{i,j \in \{1,\ldots,n\}} \mathbf{A}_{i,j} \cdot \mathbf{P}_{i,k} \cdot \mathbf{P}_{j,l} = (\mathbf{P}_{(:,k)})^T \mathbf{A} \mathbf{P}_{(:,l)},$$

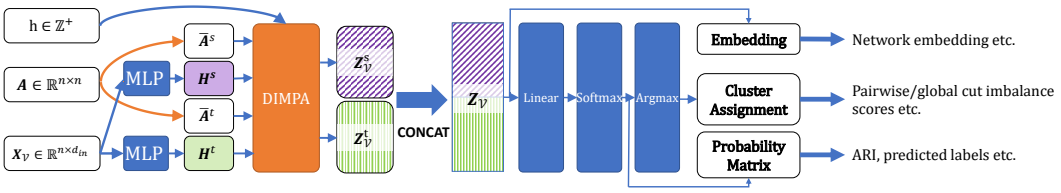

Figure 2: DIGRAC overview: from feature matrix $\mathbf{X}_{\mathcal{V}}$ and adjacency matrix $\mathbf{A}$, we first compute the row-normalized adjacency matrices $\overline{\mathbf{A}}^s$ and $\overline{\mathbf{A}}^t$. Then, we apply two separate MLPs on $\mathbf{X}_{\mathcal{V}}$, to obtain hidden representations $\mathbf{H}^s$ and $\mathbf{H}^t$. Next, we compute their decoupled embeddings using Eq. (1), and its equivalent for target embeddings. The concatenated decoupled embeddings are the final embeddings. For node clustering tasks, we add a linear layer followed by a unit *softmax* to obtain the probability matrix $\mathbf{P}$. Applying *argmax* on each row of $\mathbf{P}$ yields node cluster assignments.

Algorithm 1: Weighted Multi-Hop Neighbor Aggregation (DIMPA).

Input : (Sparse) row-normalized adjacency matrices $\overline{\mathbf{A}}^s, \overline{\mathbf{A}}^t$; initial hidden representations $\mathbf{H}^s, \mathbf{H}^t$; hop $h (h \geq 2)$; lists of scalar weights $\Omega^s = (\omega^s_{\mathbf{M}}, \mathbf{M} \in \mathcal{A}^{s,h}), \Omega^t = (\omega^t_{\mathbf{M}}, \mathbf{M} \in \mathcal{A}^{t,h})$.

Output : Vector representations $\mathbf{z}_i$ for all $v_i \in \mathcal{V}$ given by $\mathbf{Z}$.

$\tilde{\mathbf{X}}^s \leftarrow \overline{\mathbf{A}}^s \mathbf{H}^s$; $\quad$ $\tilde{\mathbf{X}}^t \leftarrow \overline{\mathbf{A}}^t \mathbf{H}^t$;

$\mathbf{Z}^s \leftarrow \Omega^s[0] \cdot \mathbf{H}^s + \Omega^s[1] \cdot \tilde{\mathbf{X}}^s$; $\quad$ $\mathbf{Z}^t \leftarrow \Omega^t[0] \cdot \mathbf{H}^t + \Omega^t[1] \cdot \tilde{\mathbf{X}}^t$;

for $i \leftarrow 2$ **to** h **do**

  $\tilde{\mathbf{X}}^s \leftarrow \overline{\mathbf{A}}^s \tilde{\mathbf{X}}^s$; $\quad$ $\tilde{\mathbf{X}}^t \leftarrow \overline{\mathbf{A}}^t \tilde{\mathbf{X}}^t$;

  $\mathbf{Z}^s \leftarrow \mathbf{Z}^s + \Omega^s[i] \cdot \tilde{\mathbf{X}}^s$; $\quad$ $\mathbf{Z}^t \leftarrow \mathbf{Z}^t + \Omega^t[i] \cdot \tilde{\mathbf{X}}^t$;

end

$\mathbf{Z} = \text{CONCAT}\,(\mathbf{Z}^s, \mathbf{Z}^t)$;

where $\mathbf{P}_{(:,k)}, \mathbf{P}_{(:,l)}$ denote the k^{th} and l^{th} columns of the assignment probability matrix $\mathbf{P}$, respectively.

• The **imbalance flow** between clusters $\mathcal{C}_k$ and $\mathcal{C}_l$ is defined as

$$|W(\mathcal{C}_k, \mathcal{C}_l) - W(\mathcal{C}_l, \mathcal{C}_k)|, \quad \forall k, l \in \{0, \ldots, K-1\}.$$

For interpretability and ease of comparison, we normalize the imbalance flows to obtain an imbalance score with values in $[0, 1]$ as follows (we defer additional details to SI A.1).

• The **probabilistic volume** for cluster $\mathcal{C}_k$ is defined as

$$VOL(\mathcal{C}_k) = VOL^{(\text{out})}(\mathcal{C}_k) + VOL^{(\text{in})}(\mathcal{C}_k) = \sum_{i,j} (\mathbf{A}_{i,j} + \mathbf{A}_{j,i}) \cdot \mathbf{P}_{j,k}.$$

Then $VOL(\mathcal{C}_k) \geq W(\mathcal{C}_k, \mathcal{C}_l)$ for all $l \in \{0, \ldots, K-1\}$ and

$$\min(VOL(\mathcal{C}_k), VOL(\mathcal{C}_l)) \geq \max(W(\mathcal{C}_k, \mathcal{C}_l), W(\mathcal{C}_l, \mathcal{C}_k)) \geq |W(\mathcal{C}_k, \mathcal{C}_l) - W(\mathcal{C}_l, \mathcal{C}_k)|. \tag{2}$$

The imbalance term, which is used in most of our experiments, denoted $\text{CI}^{\text{vol\_sum}}$, is defined as

$$\text{CI}^{\text{vol\_sum}}(k, l) = 2\frac{|W(\mathcal{C}_k, \mathcal{C}_l) - W(\mathcal{C}_l, \mathcal{C}_k)|}{VOL(\mathcal{C}_k) + VOL(\mathcal{C}_l)} \in [0, 1]. \tag{3}$$

The aim is then to find a partition which maximizes the imbalance flow, to capture groups of nodes which would represent clusters in the meta-graph. The normalization by the volumes is carried out to penalize partitions that put most nodes into a single cluster. The range $[0, 1]$ follows from Eq. (2). Additional variants are discussed in SI A.2.

To obtain a **global probabilistic imbalance score**, based on $\text{CI}^{\text{vol\_sum}}$ from Eq. (3), we average over pairwise imbalance scores of different pairs of clusters. Since the scores discussed are symmetric and the cut difference before taking absolute value is skew-symmetric, we only need to consider the pairs $\mathcal{T} = \{(\mathcal{C}_k, \mathcal{C}_l) : 0 \leq k < l \leq K-1, k, l \in \mathbb{Z}\}$. We consider a "*sort*" variant to select these pairs; concretely, we choose the pairs of clusters with the largest β pairwise cut flow imbalance

values, where β is half of the number of nonzero entries in the off-diagonal entries of the meta-graph adjacency matrix $\mathbf{F}$ (if the meta-graph is known), or can be approximated otherwise. With $\mathcal{T}(\beta) = \{(\mathcal{C}_k, \mathcal{C}_l) \in \mathcal{T} : \text{CI}^{\text{vol\_sum}}(k,l) \text{ is among the top } \beta \text{ values}\}$, where $1 \leq \beta \leq \binom{K}{2}$, we set

$$\mathcal{O}^{\text{sort}}_{\text{vol\_sum}} = \frac{1}{\beta} \sum_{(\mathcal{C}_k, \mathcal{C}_l) \in \mathcal{T}(\beta)} \text{CI}^{\text{vol\_sum}}(k,l), \quad \text{and} \quad \mathcal{L}^{\text{sort}}_{\text{vol\_sum}} = 1 - \mathcal{O}^{\text{sort}}_{\text{vol\_sum}}, \tag{4}$$

as the corresponding loss function. For example, for a "*cycle*" meta-graph with three clusters and no ambient nodes, we have $\beta = 3$. When we consider a path meta-graph with three clusters and ambient nodes, we have $\beta = 1$. Definitions of meta-graph structures are discussed in Section 4.1. In SI A.3, additional variants for selecting pairs of clusters in $\mathcal{T}$ are considered, including an "*std*" variant based on hypothesis testing, and a "*naive*" variant which includes all pairs in $\mathcal{T}$. The corresponding scores and loss functions for these variants are defined analogously.

4 Experiments

In this section, we describe the synthetic and real world data sets used in this study, and illustrate the efficacy of our method. When ground truth is available, performance is measured by the Adjusted Rand Index (ARI) [21] for node clustering, and by accuracy for node classification and link direction prediction. When no ground truth labels are given, performance is measured in terms of cut imbalance. Implementation details are provided in SI B.

In our experiments, we compare DIGRAC against the most recent related methods from the literature, able to handle directed graphs. The **ten** baselines are • (1) Bibliometric and • (2) Degree-discounted introduced in [39], • (3) DI_SIM [38], • (4) Herm and • (5) Herm_sym introduced in [12], • (6) MagNet [45], • (7) DGCN [43], • (8) three variants of DiGCN [42]. The abbreviations of these methods, when reported in the numerical experiments, are Bi_sym, DD_sym, DISG_LR, Herm, Herm_sym, MagNet, DGCN, DiGCN, DiGCN_app, DiGCN_ib, respectively. DGCN is the least efficient method in terms of speed and space complexity, followed by DiGCN_ib which involves the so-called *inception blocks* (hence the suffix *ib*). DiGCN denotes the method without using approximate Laplacian based on personalized PageRank, while DiGCN_app and DiGCN_ib use this approximation. We use the same hyperparameter settings stated in these papers. Data splits for all models are the same; methods (6), (7), (8) are trained with 80% nodes under label supervision. For MagNet, we use $q = 0.25$ for the phase matrix, as this value is predominantly used in their paper.

4.1 Data sets

Synthetic data: Directed Stochastic Block Models A standard directed stochastic blockmodel (DSBM) is often used to represent a network cluster structure, see for example [30]. Its parameters are the number K of clusters and the edge probabilities; given the cluster assignment of the nodes, the edge indicators are independent. The DSBMs used in our experiments also depend on a meta-graph adjacency matrix $\mathbf{F} = (\mathbf{F}_{k,l})_{k,l=0,\ldots,K-1}$ and a *filled* version of it, $\tilde{\mathbf{F}} = (\tilde{\mathbf{F}}_{k,l})_{k,l=0,\ldots,K-1}$, and on a noise level parameters $\eta \leq 0.5$. The meta-graph adjacency matrix $\mathbf{F}$ is generated from the given meta-graph structure, called $\mathcal{M}$. To include an ambient background, the filled meta-graph adjacency matrix $\tilde{\mathbf{F}}$ replaces every zero in $\mathbf{F}$ that is not part of the imbalance structure by 0.5.The filled meta-graph thus creates a number of *ambient nodes* which correspond to entries which are not part of $\mathcal{M}$ and thus are not part of a meaningful cluster; this set of *ambient nodes* is also called the *ambient cluster*. First, we provide examples of structures of $\mathbf{F}$ without any ambient nodes, where $\mathbb{1}$ denotes the indicator function.

• (1) "*cycle*": $\mathbf{F}_{k,l} = (1-\eta)\mathbb{1}(l = ((k+1) \mod K)) + \eta\mathbb{1}(l = ((k-1) \mod K)) + \frac{1}{2}\mathbb{1}(l = k)$.

• (2) "*path*": $\mathbf{F}_{k,l} = (1-\eta)\mathbb{1}(l = k+1) + \eta\mathbb{1}(l = k-1) + \frac{1}{2}\mathbb{1}(l = k)$.

• (3) "*complete*": assign diagonal entries $\frac{1}{2}$. For each pair (k,l) with $k < l$, let $\mathbf{F}_{k,l}$ be η and $1-\eta$ with equal probability, then assign $\mathbf{F}_{l,k} = 1 - \mathbf{F}_{k,l}$.

• (4) "*star*", following [16]: select the center node as $\omega = \lfloor \frac{K-1}{2} \rfloor$ and set $\mathbf{F}_{k,l} = (1-\eta)\mathbb{1}(k = \omega, l \text{ odd}) + \eta\mathbb{1}(k = \omega, l \text{ even}) + (1-\eta)\mathbb{1}(l = \omega, k \text{ odd}) + \eta\mathbb{1}(l = \omega, l \text{ even})$.

When ambient nodes are present, the construction involves two steps, with the first step the same as the above, but with the following changes: For "*cycle*" meta-graph structure, $\mathbf{F}_{k,l} = (1-\eta)\mathbb{1}(l = ((k+1) \mod (K-1))) + \eta\mathbb{1}(l = ((k-1) \mod (K-1))) + \frac{1}{2}\mathbb{1}(l = k)$. The second step is to assign 0 (0.5, resp.) to the last row and the last column of $\mathbf{F}$ ($\tilde{\mathbf{F}}$, resp.).

In our experiments, we choose the number of clusters, the (approximate) ratio, ρ, between the largest and the smallest cluster size, and the number, n, of nodes. To tackle the hardest clustering task, all pairs of nodes within a cluster and all pairs of nodes between clusters have the same edge probability, p. Note that for $\mathcal{M}$ ="*cycle*", even the expected in-degree and out-degree of all nodes are identical.

Our DSBM, which we denote by DSBM $(\mathcal{M}, \mathbb{1}(\text{ambient}), n, K, p, \rho, \eta)$, is built similarly to [12] but with possibly unequal cluster sizes: • (1) Assign cluster sizes $n_0 \leq n_1 \leq \cdots \leq n_{K-1}$ with size ratio $\rho \in [0, 1]$, as follows. If $\rho = 1$ then the first $K-1$ clusters have the same size $\lfloor n/K \rfloor$ and the last cluster has size $n-(K-1)\lfloor n/K \rfloor$. If $\rho > 1$, we set $\rho_0 = \rho^{\frac{1}{K-1}}$. Solving $\sum_{i=0}^{K-1} \rho_0^i n_0 = n$ and taking integer value gives $n_0 = \left\lfloor n(1-\rho_0)/(1-\rho_0^K) \right\rfloor$. Further, set $n_i = \lfloor \rho_0 n_{i-1} \rfloor$, for $i = 1, \cdots, K-2$ if $K \geq 3$, and $n_{K-1} = n - \sum_{i=0}^{K-2} n_i$. Then the ratio of the size of the largest to the smallest cluster is approximately $\rho_0^{K-1} = \rho$. • (2) Assign each node randomly to one of K clusters, so that each cluster has the allocated size. • (3) For node $v_i, v_j \in \mathcal{C}_k$, independently sample an edge from node v_i to node v_j with probability $p \cdot \tilde{\mathbf{F}}_{k,k}$. • (4) For each pair of different clusters $\mathcal{C}_k, \mathcal{C}_l$ with $k \neq l$, for each node $v_i \in \mathcal{C}_k$, and each node $v_j \in \mathcal{C}_l$, independently sample an edge from node v_i to node v_j with probability $p \cdot \tilde{\mathbf{F}}_{k,l}$. The parameter settings in our experiments are $p \in \{0.001, 0.01, 0.02, 0.1\}$, $\rho \in \{1, 1.5\}$, $K \in \{3, 5, 10\}$, $\mathbb{1}(\text{ambient}) \in \{\text{T}, \text{F}\}$ (True and False), $n \in \{1000, 5000, 30000\}$, and we also vary the direction flip probability η from 0 to 0.45, with a 0.05 step size.

Figures 1(c-d) display a "*cycle*" meta-graph structure with ambient nodes (in cluster 4). The majority (75%) of edges flow in the form $0 \to 1 \to 2 \to 3 \to 0$, while 25% flow from the opposite direction. Figure 1(d) illustrate the meta-graph adjacency matrix corresponding to $\mathbf{F}$ shown in Figure 1(c).

Real data We perform experiments on six real-world directed network data sets, namely *Telegram* [5], *Blog* [1], *Migration* [36], *WikiTalk* [27], *Cora-ML*, and *CiteSeer* [4], with more details provided in SI B.3. We use the first four data sets on node clustering tasks, and the rest for application to node classification and link direction prediction. We set the number of clusters K to be 4, 2, 10, 10, 7, 6, respectively, and values of β to be 5, 1, 9, 10, 11, 9, respectively.

4.2 Experimental results

Training set-up and hyperparameter selection As training setup, we use 10% of all nodes from each cluster as test nodes, 10% as validation nodes to select the model, and the remaining 80% as training nodes. In each setting, unless otherwise stated, we carry out 10 experiments with different data splits. Error bars are given by one standard error. Without node attributes, the matrix $\mathbf{X}_{\mathcal{V}}$ for DIGRAC is taken as the stacked eigenvectors corresponding to the largest K eigenvalues of the random-walk symmetrized Hermitian matrix used in the comparison method Herm_rw. The imbalance loss function acts on the subgraph induced by the training nodes.

Hyperparameter selection is done via greedy search, with more details in SI B.4. Figure 3(a) compares the performance of DIGRAC on DSBM with $n = 1000$ nodes, $K = 5$ clusters, $\rho = 1, p = 0.02$ without ambient nodes, under different hyperparameter settings. We remark that hop $h = 2$ should be chosen in order to reduce complexity, as increasing h does not lead to increased performance. Therefore, our default setting is hop $h = 2, d = 32, \tau = 0.5$.

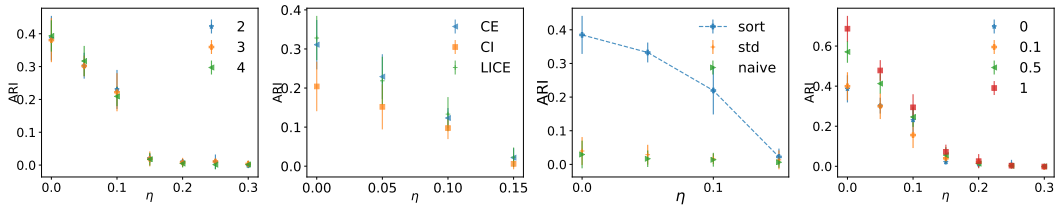

(a) Vary the hop h in DIMPA. (b) Vary loss for DiGCN: CE, CI or LICE. (c) Vary selection methods of imbalance pairs. (d) Vary seed ratio in a semi-supervised setting.

Figure 3: Hyperparemter analysis (a) and ablation study (b-d) on a "*cycle*" DSBM with $n = 1000$ nodes, $K = 5$ clusters, $\rho = 1$, and $p = 0.02$, without ambient nodes.

Node clustering results on synthetic data Figure 4 compares the numerical performance of DIGRAC with other methods on synthetic data. For this figure we generate 5 DSBM networks under each parameter setting and use 10 different data splits for each network, then average over the 50 runs. Error bars are given by one standard error. Additional implementation details are available in SI B.

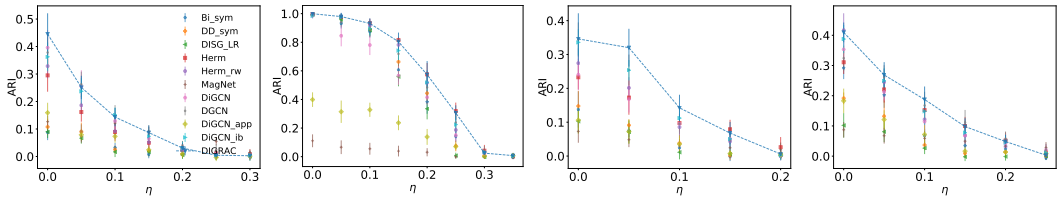

(a) DSBM("complete", T, $n = 1000, K = 10, p = 0.02, \rho = 1$)

(b) DSBM("cycle", F, $n = 1000, K = 3, p = 0.02, \rho = 1.5$)

(c) DSBM("path", F, $n = 1000, K = 5, p = 0.02, \rho = 1$)

(d) DSBM("star", F, $n = 1000, K = 5, p = 0.02, \rho = 1$)

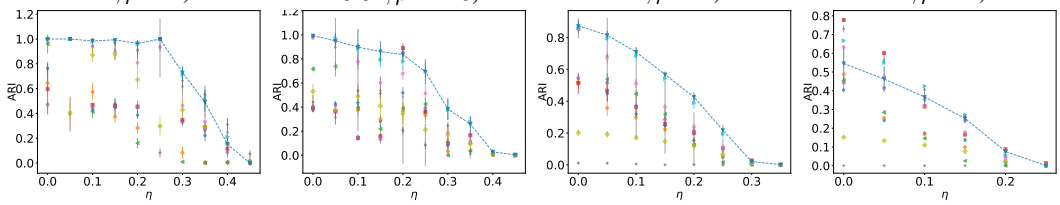

(e) DSBM("complete", F, $n = 1000, K = 3, p = 0.1, \rho = 1$)

(f) DSBM("complete", T, $n = 1000, K = 5, p = 0.1, \rho = 1.5$)

(g) DSBM("cycle", T, $n = 5000, K = 5, p = 0.01, \rho = 1.5$)

(h) DSBM("cycle", F, $n = 30000, K = 5, p = 0.001, \rho = 1$)

Figure 4: Node clustering test ARI comparison on synthetic data. Dashed lines highlight DIGRAC's performance. Error bars are given by one standard error.

Table 1: Performance comparison on real data sets. The best is marked in **bold red** and the second best is marked in underline blue. The objectives are defined in Section 3.3.

Metric	Data set	Bi_sym	DD_sym	DISG_LR	Herm	Herm_rw	DIGRAC
$\mathcal{O}^{\text{sort}}_{\text{vol\_sum}}$	*Telegram*	0.21±0.0	0.21±0.0	0.21±0.01	0.2±0.01	0.14±0.0	**0.32±0.01**
	Blog	0.07±0.0	0.0±0.0	0.05±0.0	0.37±0.0	0.0±0.0	**0.44±0.0**
	Migration	0.03±0.0	0.01±0.0	0.01±0.0	**0.07±0.0**	0.01±0.0	0.04±0.0
	WikiTalk	N/A	N/A	0.18±0.03	0.15±0.02	0.0±0.0	**0.24±0.05**
$\mathcal{O}^{\text{naive}}_{\text{vol\_sum}}$	*Telegram*	0.26±0.0	0.26±0.0	0.26±0.01	0.25±0.02	0.23±0.0	**0.27±0.01**
	Blog	0.07±0.0	0.0±0.0	0.05±0.0	0.37±0.0	0.0±0.0	**0.44±0.0**
	Migration	0.01±0.0	0.0±0.0	0.0±0.0	0.02±0.0	0.0±0.0	**0.03±0.01**
	WikiTalk	N/A	N/A	0.1±0.02	0.04±0.0	0.0±0.0	**0.12±0.01**

We conclude that DIGRAC attains state-of-the-art results on a wide range of network densities and noise levels, on different network sizes, and with different meta-graph structures, whether or not there exist ambient nodes. DIGRAC outperforms its competitors by a large margin especially when there exist ambient nodes, which validates its strength of extracting the main directional signal planted in a larger graph. Additional results are reported in SI C, from which similar conclusions can be drawn.

Node clustering results on real data For our four real data sets, the node in- and out-degrees may not be identical across clusters. Moreover, as these data sets do not contain node attributes, DIGRAC considers the eigenvectors corresponding to the largest K eigenvectors of the Hermitian matrix from [12] to construct an input feature matrix. Table 1 reveals that DIGRAC provides competitive global imbalance scores in both objectives discussed and across all real data sets, and outperforms all other methods in 7 out of 8 instances, on the four data sets and two objective functions, and only once it places second, after Herm. The N/A entries in the table are caused by memory error. The experiments indicated that edge directionality can contain an important signal that DIGRAC is able to capture. A comprehensive numerical comparison is available in SI D, revealing similar conclusions.

Application to node classification and link direction prediction As a secondary use case for our imbalance loss function, we compare performance on *node classification* and *link direction prediction* on two benchmark data sets. For *node classification*, we use the same data splits and input features as [42], 20 training nodes in each class, 500 validation nodes in total at random, and the rest as test nodes. We compare the GNN baselines with their respective variants employing as loss the sum of cross entropy loss (baseline) and $\mathcal{L}^{\text{sort}}_{\text{vol\_sum}}$; we call this sum the *Loss Imbalance Cross Entropy (LICE)*. The imbalance loss is applied to the subgraph induced by training nodes, while the cross-entropy loss is applied to all training nodes. For this task, we compare performance on DiGCN and DiGCN_ib.

Table 2: Node classification (top) and link direction prediction (bottom) test accuracy (%) on real data sets. Ending "+LI" indicates using the sum of cross-entropy loss and $\mathcal{L}^{\text{sort}}_{\text{vol\_sum}}$ as the loss (LICE).

Task	Data set	DiGCN	DiGCN+LI	Avg. gain	DiGCN_ib	DiGCN_ib+LI	Avg. gain
node classification	*Cora-ML*	37.55 ± 5.17	38.89 ± 5.20	1.34	74.59 ± 2.84	75.14 ± 2.89	0.55
	CiteSeer	31.89 ± 3.87	32.06 ± 3.43	0.17	37.33 ± 9.14	39.60 ± 8.14	2.28
Task	Data set	DGCN	DGCN+LI	Avg. gain	DiGCN_app	DiGCN_app+LI	Avg. gain
link direction prediction	*Cora-ML*	81.97 ± 4.70	83.77 ± 1.01	1.80	75.27 ± 9.22	80.89 ± 3.59	5.62
	CiteSeer	81.04 ± 10.39	84.49 ± 1.73	3.45	71.59 ± 10.88	77.28 ± 2.11	5.69

Link direction prediction corresponds to a binary classification problem for edges (forward and backward direction), assuming absence of edges in both directions. We use 80% of all edges to train, 15% to test, and 5% for validation. We compare the performance of using only cross-entropy loss to using LICE as loss in DGCN and DiGCN_app for link direction prediction. For both tasks, we use the same hyperparameter settings as above, without further tuning of hyperparameters. We use the given features for node classification, and in-out degrees as features for link direction prediction.

The upper part of Table 2 shows that flow imbalance could aid node classification even when $\mathcal{L}^{\text{sort}}_{\text{vol\_sum}}$ is applied to the subgraph induced by only a small subset of all nodes, for DiGCN and DiGCN_ib. As shown in the bottom of Table 2, by applying LICE to the observed network (with only training edges), DGCN and DiGCN_app achieve on average higher test accuracy in link direction prediction on both data sets, which indicates that with some further tuning, the imbalance loss function could be a valuable addition to link direction prediction. Details and more results are discussed in SI D.5.

4.3 Ablation study

Figure 3(b) compares the performance of DiGCN replacing the loss function by $\mathcal{L}^{\text{sort}}_{\text{vol\_sum}}$ from Eq. (4), indicated by "CI", or LICE, sum of supervised and self-supervised loss, on a DSBM("*cycle*", T, $n = 1000, K = 5, p = 0.02, \rho = 1$) model. We conclude that replacing the supervised loss function with $\mathcal{L}^{\text{sort}}_{\text{vol\_sum}}$ leads to comparable results, and that adding $\mathcal{L}^{\text{sort}}_{\text{vol\_sum}}$ to the loss could be beneficial.

Figure 3(c) compares the test ARI performance using three variants of loss functions on the same digraph. The current choice "*sort*" performs best among these variants, indicating a benefit in only considering top pairs of individual imbalance scores. More details on loss functions, comparison with other variants, and evaluation on additional metrics are discussed in SI A, with similar conclusions.

As illustrated in Figure 3(d), again on the same digraph, we also experiment on adding seeds, with the seed ratio defined as the ratio of the number of seed nodes to the number of training nodes. A supervised loss, following [41], is then applied to these seeds; SI B.5 further elaborates on this end. In conclusion, seed nodes with a supervised loss function enhance performance, from which we infer that our model can further boost its performance when additional label information is available.

5 Conclusion, limitations and future work

DIGRAC provides an end-to-end pipeline to create node embeddings and perform directed clustering, with or without available additional node features or cluster labels. We illustrate DIGRAC on publicly available data often used as benchmarks, and without any personally identifiable information. DIGRAC could potentially have societal impact, for example, in detecting clusters of fake accounts in social networks. We do not envision our work to have any negative societal impact. Further work will include additional experiments in the semi-supervised setting, when there exist seed nodes with known cluster labels, or when additional information is available in the form of *must-link* and *cannot-link* constraints, popular in the *constrained clustering* literature [3, 9]. Another future direction pertains to extending our framework to also detect the number of clusters [37, 8], instead of specifying it a-priori, as this is typically not available in real world applications. The current framework requires additional preliminary analysis on how many pairwise imbalance scores to consider, such as by inspecting the (initial or fitted) meta-graph adjacency matrix. It would be interesting to build a more powerful framework that can automatically detect the value β used in the current model, to select the subset of influential pairs of imbalances.

Further research directions will address the performance in the sparse regime, where spectral methods are known to underperform, and various regularizations have been proven to be effective both on the theoretical and experimental fronts; for example, see regularization in the sparse regime for the

undirected settings [6, 2, 13]. Finally, adapting our pipeline for directed clustering in extremely large networks, possibly combined with sampling methods or mini-batch [19], is a direction worth exploring, rendering DIGRAC applicable to large scale industrial applications.

Acknowledgements. YH acknowledges the support of a Clarendon scholarship from the University of Oxford. GR is funded in part by by EPSRC grants EP/T018445/1 and EP/R018472/1. MC acknowledges support from the EPSRC grant EP/N510129/1 at The Alan Turing Institute.

References

[1] Lada A Adamic and Natalie Glance. The political blogosphere and the 2004 US election: divided they blog. In *Proceedings of the 3rd International Workshop on Link Discovery*, pages 36–43, 2005.

[2] Arash A. Amini, Aiyou Chen, Peter J. Bickel, and Elizaveta Levina. Pseudo-likelihood methods for community detection in large sparse networks. *The Annals of Statistics*, 41(4):2097–2122, 2013.

[3] Sugato Basu, Ian Davidson, and Kiri Wagstaff. *Constrained Clustering: Advances in Algorithms, Theory, and Applications*. CRC Press, 2008.

[4] Aleksandar Bojchevski and Stephan Günnemann. Deep Gaussian embedding of graphs: Unsupervised inductive learning via ranking. In *ICLR Workshop on Representation Learning on Graphs and Manifolds*, 2017.

[5] Alexandre Bovet and Peter Grindrod. The Activity of the Far Right on Telegram. `https://www.researchgate.net/publication/346968575_The_Activity_of_the_Far_Right_on_Telegram_v21`, 2020.

[6] Kamalika Chaudhuri, Fan Chung, and Alexander Tsiatas. Spectral clustering of graphs with general degrees in the extended planted partition model. In *25th Annual Conference on Learning Theory*, volume 23 of *Proceedings of Machine Learning Research*, pages 35.1–35.23, Edinburgh, Scotland, 2012. JMLR Workshop and Conference Proceedings.

[7] Louis HY Chen, Larry Goldstein, and Qi-Man Shao. *Normal approximation by Stein's method*. Springer Science & Business Media, 2010.

[8] Yilin Chen and Jack W Baker. Community detection in spatial correlation graphs: Application to non-stationary ground motion modeling. *Computers and Geosciences*, 2021.

[9] M. Cucuringu, I. Koutis, S. Chawla, G. Miller, and R. Peng. Scalable Constrained Clustering: A Generalized Spectral Method. *Artificial Intelligence and Statistics Conference (AISTATS) 2016*, 2016.

[10] Mihai Cucuringu. Sync-rank: Robust ranking, constrained ranking and rank aggregation via eigenvector and SDP synchronization. *IEEE Transactions on Network Science and Engineering*, 3(1):58–79, 2016.

[11] Mihai Cucuringu, Vincent Blondel, and Paul Van Dooren. Extracting spatial information from networks with low-order eigenvectors. *Phys. Rev. E*, 87:032803, Mar 2013.

[12] Mihai Cucuringu, Huan Li, He Sun, and Luca Zanetti. Hermitian matrices for clustering directed graphs: insights and applications. In *International Conference on Artificial Intelligence and Statistics*, pages 983–992. PMLR, 2020.

[13] Mihai Cucuringu, Apoorv Vikram Singh, Déborah Sulem, and Hemant Tyagi. Regularized spectral methods for clustering signed networks. *arXiv:2011.01737*, 2020.

[14] Mukeshwar Dhamala, Govindan Rangarajan, and Mingzhou Ding. Analyzing information flow in brain networks with nonparametric Granger causality. *NeuroImage*, 41(2):354–362, 2008.

[15] Andrew Elliott, Angus Chiu, Marya Bazzi, Gesine Reinert, and Mihai Cucuringu. Core–periphery structure in directed networks. *Proceedings of the Royal Society A*, 476(2241):20190783, 2020.

[16] Andrew Elliott, Paul Reidy Milton Martinez Luaces, Mihai Cucuringu, and Gesine Reinert. Anomaly detection in networks using spectral methods and network comparison approaches. *arXiv preprint arXiv:1901.00402*, 2019.

[17] Michelle Girvan and Mark EJ Newman. Community structure in social and biological networks. *Proceedings of the National Academy of Sciences*, 99(12):7821–7826, 2002.

[18] Gero Greiner and Riko Jacob. The I/O Complexity of Sparse Matrix Dense Matrix Multiplication", booktitle="LATIN 2010: Theoretical Informatics. pages 143–156, Berlin, Heidelberg, 2010. Springer Berlin Heidelberg.

[19] William L Hamilton, Rex Ying, and Jure Leskovec. Inductive representation learning on large graphs. In *Proceedings of the 31st International Conference on Neural Information Processing Systems*, pages 1025–1035, 2017.

[20] Adam P Harrison and Dileepan Joseph. High performance rearrangement and multiplication routines for sparse tensor arithmetic. *SIAM Journal on Scientific Computing*, 40(2):C258–C281, 2018.

[21] Lawrence Hubert and Phipps Arabie. Comparing partitions. *Journal of Classification*, 2(1):193–218, 1985.

[22] Caiyan Jia, Yafang Li, Matthew B Carson, Xiaoyang Wang, and Jian Yu. Node attribute-enhanced community detection in complex networks. *Scientific Reports*, 7(1):1–15, 2017.

[23] Diederik P Kingma and Jimmy Ba. Adam: A method for stochastic optimization. *arXiv preprint arXiv:1412.6980*, 2014.

[24] Thomas N Kipf and Max Welling. Semi-supervised classification with graph convolutional networks. *arXiv preprint arXiv:1609.02907*, 2016.

[25] Steinar Laenen and He Sun. Higher-order spectral clustering of directed graphs. *Advances in Neural Information Processing Systems*, 2020.

[26] Elizabeth A Leicht and Mark EJ Newman. Community structure in directed networks. *Physical Review Letters*, 100(11):118703, 2008.

[27] Jure Leskovec, Daniel Huttenlocher, and Jon Kleinberg. Signed networks in social media. In *Proceedings of the SIGCHI Conference on Human Factors in Computing Systems*, pages 1361–1370, 2010.

[28] Jure Leskovec, Kevin J Lang, Anirban Dasgupta, and Michael W Mahoney. Statistical properties of community structure in large social and information networks. In *Proceedings of the 17th International Conference on World Wide Web*, pages 695–704, 2008.

[29] Yi Ma, Jianye Hao, Yaodong Yang, Han Li, Junqi Jin, and Guangyong Chen. Spectral-based graph convolutional network for directed graphs. *arXiv preprint arXiv:1907.08990*, 2019.

[30] Fragkiskos D Malliaros and Michalis Vazirgiannis. Clustering and community detection in directed networks: A survey. *Physics reports*, 533(4):95–142, 2013.

[31] Elan Sopher Markowitz, Keshav Balasubramanian, Mehrnoosh Mirtaheri, Sami Abu-El-Haija, Bryan Perozzi, Greg Ver Steeg, and Aram Galstyan. Graph traversal with tensor functionals: A meta-algorithm for scalable learning. In *International Conference on Learning Representations*, 2021.

[32] Bojan Mohar. A new kind of Hermitian matrices for digraphs. *Linear Algebra and its Applications*, 584:343–352, 2020.

[33] Federico Monti, Karl Otness, and Michael M. Bronstein. Motifnet: A motif-based graph convolutional network for directed graphs. In *2018 IEEE Data Science Workshop (DSW)*, pages 225–228, 2018.

[34] Mark EJ Newman. Modularity and community structure in networks. *Proceedings of the National Academy of Sciences*, 103(23):8577–8582, 2006.

[35] William R. Palmer and Tian Zheng. Spectral clustering for directed networks. In Rosa M. Benito, Chantal Cherifi, Hocine Cherifi, Esteban Moro, Luis Mateus Rocha, and Marta Sales-Pardo, editors, *Complex Networks & Their Applications IX*, pages 87–99, Cham, 2021. Springer International Publishing.

[36] Marc J Perry. *State-to-state Migration Flows, 1995 to 2000*. US Department of Commerce, Economics and Statistics Administration, US, 2003.

[37] Maria A Riolo, George T Cantwell, Gesine Reinert, and Mark EJ Newman. Efficient method for estimating the number of communities in a network. *Physical Review E*, 96(3):032310, 2017.

[38] Karl Rohe, Tai Qin, and Bin Yu. Co-clustering directed graphs to discover asymmetries and directional communities. *Proceedings of the National Academy of Sciences*, 113(45):12679–12684, 2016.

[39] Venu Satuluri and Srinivasan Parthasarathy. Symmetrizations for clustering directed graphs. In *Proceedings of the 14th International Conference on Extending Database Technology*, pages 343–354, 2011.

[40] Ali Shojaie and Emily B Fox. Granger causality: A review and recent advances. *arXiv preprint arXiv:2105.02675*, 2021.

[41] Yu Tian, Long Zhao, Xi Peng, and Dimitris N Metaxas. Rethinking kernel methods for node representation learning on graphs. *Advances in Neural Information Processing Systems*, 32, 2019.

[42] Zekun Tong, Yuxuan Liang, Changsheng Sun, Xinke Li, David Rosenblum, and Andrew Lim. Digraph inception convolutional networks. *Advances in Neural Information Processing Systems*, 33, 2020.

[43] Zekun Tong, Yuxuan Liang, Changsheng Sun, David S Rosenblum, and Andrew Lim. Directed graph convolutional network. *arXiv preprint arXiv:2004.13970*, 2020.

[44] Jingnan Zhang, Xin He, and Junhui Wang. Directed community detection with network embedding. *Journal of the American Statistical Association*, pages 1–11, 2021.

[45] Xitong Zhang, Nathan Brugnone, Michael Perlmutter, and Matthew Hirn. MagNet: A Magnetic Neural Network for Directed Graphs. *arXiv preprint arXiv:2102.11391*, 2021.

A Loss and objectives

A.1 Additional details on probabilistic cut and volume

Recall that the **probabilistic cut** from cluster $\mathcal{C}_k$ to $\mathcal{C}_l$ is defined as

$$W(\mathcal{C}_k, \mathcal{C}_l) = \sum_{i,j \in \{1,\dots,n\}} \mathbf{A}_{i,j} \cdot \mathbf{P}_{i,k} \cdot \mathbf{P}_{j,l} = (\mathbf{P}_{(:,k)})^T \mathbf{A} \mathbf{P}_{(:,l)},$$

where $\mathbf{P}_{(:,k)}, \mathbf{P}_{(:,l)}$ denote the k^{th} and l^{th} columns of the assignment probability matrix $\mathbf{P}$, respectively. The **imbalance flow** between clusters $\mathcal{C}_k$ and $\mathcal{C}_l$ is defined as

$$|W(\mathcal{C}_k, \mathcal{C}_l) - W(\mathcal{C}_l, \mathcal{C}_k)|,$$

for $k, l \in \{0, \dots, K-1\}$. The loss functions proposed in the main paper can be understood in terms of a probabilistic notion of degrees, as follows. We define the probabilistic out-degree of node v_i with respect to cluster k by $\tilde{d}^{(\text{out})}_{i,k} = \sum_{j=1}^{n} \mathbf{A}_{i,j} \cdot \mathbf{P}_{j,k} = \left(\mathbf{A}\mathbf{P}_{(:,k)}\right)_i$, where subscript i refers to the i^{th} entry of the vector $\mathbf{A}\mathbf{P}_{(:,k)}$. Similarly, we define the probabilistic in-degree of node v_i with respect to cluster k by $\tilde{d}^{(\text{in})}_{i,k} = \left(\mathbf{A}^T\mathbf{P}_{(:,k)}\right)_i$, where $\mathbf{A}^T$ is the transpose of $\mathbf{A}$. The **probabilistic degree** of node v_i with respect to cluster k is $\tilde{d}_{i,k} = \tilde{d}^{(\text{in})}_{i,k} + \tilde{d}^{(\text{out})}_{i,k} = \left((\mathbf{A}^T + \mathbf{A})\mathbf{P}_{(:,k)}\right)_i = \sum_{j=1}^{n} (\mathbf{A}_{i,j} + \mathbf{A}_{j,i}) \cdot \mathbf{P}_{j,k}$.

For comparisons and ease of interpretation, it is advantageous to normalize the imbalance flow between clusters; for this purpose, we introduce the probabilistic volume of a cluster, as follows. The *probabilistic out-volume* for cluster $\mathcal{C}_k$ is defined as $VOL^{(\text{out})}(\mathcal{C}_k) = \sum_{i,j} \mathbf{A}_{j,i} \cdot \mathbf{P}_{j,k}$, and the *probabilistic in-volume* for cluster $\mathcal{C}_k$ is defined as $VOL^{(\text{in})}(\mathcal{C}_k)(\mathbf{A}^T\mathbf{P}_{(:,k)})_i$, where $\mathbf{A}^T$ is the transpose of $\mathbf{A}$. These volumes can be viewed as sum of probabilistic out-degrees and in-degrees, respectively; for example, $VOL^{(\text{in})}(\mathcal{C}_k) = \sum_{i=1}^{n} \tilde{d}^{(\text{in})}_{i,k}$. Then, it holds true that

$$VOL^{(\text{out})}(\mathcal{C}_k) = \sum_{i,j} \mathbf{A}_{i,j} \cdot \mathbf{P}_{i,k} \geq \sum_{i,j} \mathbf{A}_{i,j} \cdot \mathbf{P}_{i,k} \cdot \mathbf{P}_{j,l} = W(\mathcal{C}_k, \mathcal{C}_l), \tag{5}$$

since entries in $\mathbf{P}$ are probabilities, which are in $[0, 1]$, and all entries of $\mathbf{A}$ are nonnegative. Similarly, $VOL^{(\text{in})}(\mathcal{C}_k) \geq W(\mathcal{C}_l, \mathcal{C}_k)$.

The **probabilistic volume** for cluster $\mathcal{C}_k$ is defined as

$$VOL(\mathcal{C}_k) = VOL^{(\text{out})}(\mathcal{C}_k) + VOL^{(\text{in})}(\mathcal{C}_k) = \sum_{i,j} (\mathbf{A}_{i,j} + \mathbf{A}_{j,i}) \cdot \mathbf{P}_{j,k}.$$

Then, it holds true that $VOL(\mathcal{C}_k) \geq W(\mathcal{C}_k, \mathcal{C}_l)$ for all $l \in \{0, \dots, K-1\}$ and

$$\min(VOL(\mathcal{C}_k), VOL(\mathcal{C}_l)) \geq \max(W(\mathcal{C}_k, \mathcal{C}_l), W(\mathcal{C}_l, \mathcal{C}_k)) \geq |W(\mathcal{C}_k, \mathcal{C}_l) - W(\mathcal{C}_l, \mathcal{C}_k)|. \tag{6}$$

When there exists a strong imbalance, then $|W(\mathcal{C}_k, \mathcal{C}_l) - W(\mathcal{C}_l, \mathcal{C}_k)| \approx \max(W(\mathcal{C}_k, \mathcal{C}_l), W(\mathcal{C}_l, \mathcal{C}_k))$. As an extreme case, if $\mathbf{P}_{j,l} = 1$ for all nonnegative terms in the summations in Eq. (5), and $VOL^{(\text{in})}(\mathcal{C}_k) = 0$, then $|W(\mathcal{C}_k, \mathcal{C}_l) - W(\mathcal{C}_l, \mathcal{C}_k)| = VOL(\mathcal{C}_k)$.

A.2 Variants of normalization

Recall that the imbalance term involved in most of our experiments, named $\text{CI}^{\text{vol\_sum}}$, is defined as

$$\text{CI}^{\text{vol\_sum}}(k, l) = 2\frac{|W(\mathcal{C}_k, \mathcal{C}_l) - W(\mathcal{C}_l, \mathcal{C}_k)|}{VOL(\mathcal{C}_k) + VOL(\mathcal{C}_l)} \in [0, 1]. \tag{7}$$

An alternative, which does not take volumes into account, is given by

$$\text{CI}^{\text{plain}}(k, l) = \left|\frac{W(\mathcal{C}_k, \mathcal{C}_l) - W(\mathcal{C}_l, \mathcal{C}_k)}{W(\mathcal{C}_k, \mathcal{C}_l) + W(\mathcal{C}_l, \mathcal{C}_k)}\right| = 2\left|\frac{W(\mathcal{C}_k, \mathcal{C}_l)}{W(\mathcal{C}_k, \mathcal{C}_l) - W(\mathcal{C}_l, \mathcal{C}_k)} - \frac{1}{2}\right| \in [0, 1]. \tag{8}$$

We call this cut flow imbalance CI^{plain} as it does not penalize extremely unbalanced cluster sizes.

To achieve balanced cluster sizes and still constrain each imbalance term to be in $[0, 1]$, one solution is to multiply the imbalance flow value by the minimum of $VOL(\mathcal{C}_k)$ and $VOL(\mathcal{C}_l)$, and then divide by

$\max_{(k',l')\in\mathcal{T}}(\min(VOL(\mathcal{C}_{k'}), VOL(\mathcal{C}_{l'})))$, where $\mathcal{T} = \{(\mathcal{C}_k, \mathcal{C}_l) : 0 \le k < l \le K-1, k, l \in \mathbb{Z}\}$. The reason for using $\mathcal{T}$ is that $\text{CI}^{\text{plain}}(k,l)$ is symmetric with respect to k and l, and $\text{CI}^{\text{plain}}(k,l) = 0$ whenever $k = l$. Note that the maximum of the minimum here equals the second largest volume among clusters. We then obtain $\text{CI}^{\text{vol\_min}}$ as

$$\text{CI}^{\text{vol\_min}}(k,l) = \text{CI}^{\text{plain}}(k,l) \times \frac{\min(VOL(\mathcal{C}_k), VOL(\mathcal{C}_l))}{\max_{(k',l')\in\mathcal{T}}(\min(VOL(\mathcal{C}_{k'}), VOL(\mathcal{C}_{l'})))}. \tag{9}$$

Another potential choice, denoted $\text{CI}^{\text{vol\_max}}$, whose normalization follows from the same reasoning as $\text{CI}^{\text{vol\_sum}}$, is given by

$$\text{CI}^{\text{vol\_max}}(k,l) = \frac{|W(\mathcal{C}_k, \mathcal{C}_l) - W(\mathcal{C}_l, \mathcal{C}_k)|}{\max(VOL(\mathcal{C}_k), VOL(\mathcal{C}_l))} \in [0,1]. \tag{10}$$

A.3 Variants of choosing the pairwise imbalance scores

We consider three variants for choosing the cluster pairs.
• (1) The ***"sort"*** variant picks the largest β pairwise cut imbalance values, where β is half of the number of nonzero entries in the off-diagonal entries of the meta-graph adjacency matrix $\mathbf{F}$, if the meta-graph is known or can be approximated. For example, when we have a "cycle" meta-graph with three clusters and no ambient nodes, then $\beta = 3$. When we have a "path" meta-graph with three clusters and ambient nodes, then $\beta = 1$.
• (2) The ***"naive"*** variant considers all possible $\binom{K}{2}$ pairwise cut imbalance values.
• (3) The ***"std"*** variant only considers pairwise cut imbalance values that are 3 standard deviations away from the imbalance values; the standard deviation is calculated under the null hypothesis that the between-cluster relationship has no direction preference, i.e. $\mathbf{F}_{k,l} = \mathbf{F}_{l,k}$, as follows.

Suppose two clusters have only noisy links between them (no edge in the meta-graph $\mathbf{F}$). Suppose also that the underlying network is fixed in terms of the number of nodes and where edges exist; the only randomness stems from the direction of an edge. Then, for each edge between these two clusters, say, clusters $\mathcal{C}_k$ and $\mathcal{C}_l$, the edge direction is random, i.e. the edge is from $\mathcal{C}_k$ to $\mathcal{C}_l$ with probability 0.5, and $\mathcal{C}_l$ to $\mathcal{C}_k$ with probability 0.5 also. Let $\mathcal{E}^{k,l}$ denote the set of edges between $\mathcal{C}_k$ and $\mathcal{C}_l$ if $\mathcal{E}^{k,l}$ is not empty, then for every edge $e \in \mathcal{E}^{k,l}$, define a Rademacher random variable X_e by

$$X_e = \begin{cases} 1 & \text{if the edge is from } \mathcal{C}_k \text{ to } \mathcal{C}_l, \\ -1, & \text{otherwise.} \end{cases} \tag{11}$$

Then $(X_e + 1)/2 \sim Ber(0.5)$ is a Bernoulli(0.5) random variable with mean $2 \times 0.5 - 1 = 0$ and variance $2^2 \times 0.5 \times (1 - 0.5) = 1$. In the case of unweighted edges, the total number of edges between $\mathcal{C}_k$ and $\mathcal{C}_l$ is $|\mathcal{E}^{k,l}| = W(\mathcal{C}_k, \mathcal{C}_l) + W(\mathcal{C}_l, \mathcal{C}_k)$, and that the sum of X_e terms is $\sum_{e\in\mathcal{E}^{k,l}} X_e = W(\mathcal{C}_k, \mathcal{C}_l) - W(\mathcal{C}_l, \mathcal{C}_k)$. In the case of weighted edges, with symmetric edge weights $w_{i,j} = w_{j,i}$ given and only edge direction random, it holds that $W(\mathcal{C}_k, \mathcal{C}_l) - W(\mathcal{C}_l, \mathcal{C}_k) = \sum_{e\in\mathcal{E}^{k,l}} X_e w_e$.

Let us assume that the edge indicators are independent and that $\sum_{e\in\mathcal{E}^{k,l}} w_e^2 > 0$. Under the null hypothesis that there is no meta-graph edge between $\mathcal{C}_k$ and $\mathcal{C}_l$, the random variable $\frac{\sum_{e\in\mathcal{E}^{k,l}} X_e w_e}{\sqrt{\sum_{e\in\mathcal{E}^{k,l}} w_e^2}}$ has mean 0 and variance 1. Assuming that the weights are bounded above and that $\sum_{e\in\mathcal{E}^{k,l}} w_e^2$ is bounded away from 0 with increasing network size, we can employ the Central Limit Theorem for sums of independent random variables, see for example Theorem 3.4 in [7]. Then, under the null hypothesis, approximately 99.7 % of the observations would fall within 3 standard deviations from 0. While this calculation makes many assumptions and ignores reciprocal edges, the resulting threshold is still a useful guideline for restricting attention to pairwise imbalance values which are very likely to capture a true signal.

A.4 Selection of the loss function

Table 3 provides naming conventions of all the twelve pairs of variants of objectives and loss functions used in this paper. We select the loss functions for DIGRAC based on two representative models, and compare the performance of different loss functions. We use $d = 32$, hidden units, $h = 2$ hops, and no seed nodes. Figures 5(a) and 6 compare twelve choices of loss combinations on a DSBM

Table 3: Naming conventions for objectives and loss functions

Selection variant / CI	$CI^{\text{vol\_sum}}$	$CI^{\text{vol\_min}}$	$CI^{\text{vol\_max}}$	CI^{plain}
sort	$\mathcal{O}^{\text{sort}}_{\text{vol\_sum}}, \mathcal{L}^{\text{sort}}_{\text{vol\_sum}}$	$\mathcal{O}^{\text{sort}}_{\text{vol\_min}}, \mathcal{L}^{\text{sort}}_{\text{vol\_min}}$	$\mathcal{O}^{\text{sort}}_{\text{vol\_max}}, \mathcal{L}^{\text{sort}}_{\text{vol\_max}}$	$\mathcal{O}^{\text{sort}}_{\text{plain}}, \mathcal{L}^{\text{sort}}_{\text{plain}}$
std	$\mathcal{O}^{\text{std}}_{\text{vol\_sum}}, \mathcal{L}^{\text{std}}_{\text{vol\_sum}}$	$\mathcal{O}^{\text{std}}_{\text{vol\_min}}, \mathcal{L}^{\text{std}}_{\text{vol\_min}}$	$\mathcal{O}^{\text{std}}_{\text{vol\_max}}, \mathcal{L}^{\text{std}}_{\text{vol\_max}}$	$\mathcal{O}^{\text{std}}_{\text{plain}}, \mathcal{L}^{\text{std}}_{\text{plain}}$
naive	$\mathcal{O}^{\text{naive}}_{\text{vol\_sum}}, \mathcal{L}^{\text{naive}}_{\text{vol\_sum}}$	$\mathcal{O}^{\text{naive}}_{\text{vol\_min}}, \mathcal{L}^{\text{naive}}_{\text{vol\_min}}$	$\mathcal{O}^{\text{naive}}_{\text{vol\_max}}, \mathcal{L}^{\text{naive}}_{\text{vol\_max}}$	$\mathcal{O}^{\text{naive}}_{\text{plain}}, \mathcal{L}^{\text{naive}}_{\text{plain}}$

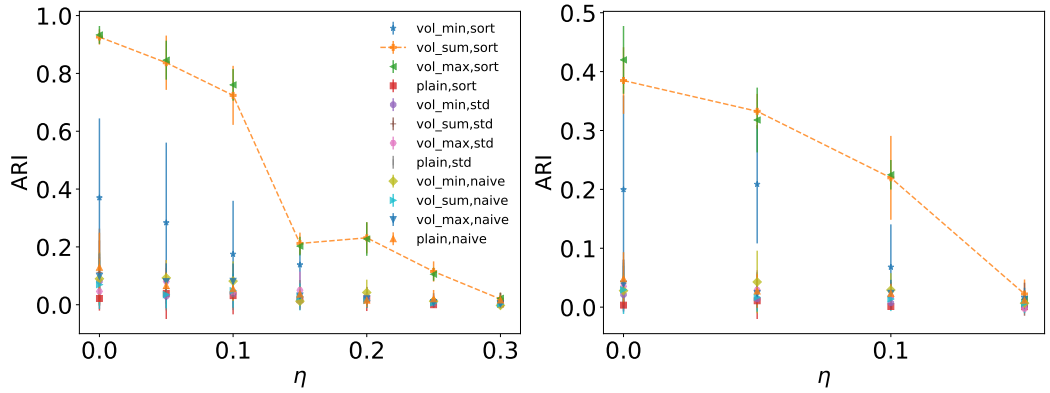

(a) DSBM("complete", F, $n = 1000, K = 5, p = 0.02, \rho = 1$)

(b) DSBM("cycle", F, $n = 1000, K = 5, p = 0.02, \rho = 1$)

Figure 5: ARI comparison of loss functions on DSBM with 1000 nodes, 5 blocks, $\rho = 1, p = 0.02$ without ambient nodes, of cycle (left) and complete (right) meta-graph structures, respectively. The first component of the legend is the choice of pairwise imbalance, and the second component is the variant of selecting pairs. The naming conventions for the abbreviations in the legend are provided in Table 3.

with $n = 1000$ nodes, $K = 5$ blocks, $\rho = 1, p = 0.02$ without ambient nodes, with a complete meta-graph structure. The subscript indicates the choice of pairwise imbalance, and the superscript indicates the variant of selecting pairs. Figures 5(b) and 7 are based on a DSBM with $n = 1000$ nodes, $K = 5$ blocks, $\rho = 1, p = 0.02$ without ambient nodes, with a cycle meta-graph structure.

These figures indicate that the "*sort*" variant generally provides the best test ARI performance and the best overall global imbalance scores, among which using normalizations $\text{CI}^{\text{vol\_sum}}$ and $\text{CI}^{\text{vol\_max}}$ perform the best. $\mathcal{L}^{\text{sort}}_{\text{vol\_min}}$ appears to behave worse than $\mathcal{L}^{\text{sort}}_{\text{vol\_sum}}$ and $\mathcal{L}^{\text{sort}}_{\text{vol\_max}}$, even when using the "sort" variant to select pairwise imbalance scores. One possible explanation is that $\mathcal{L}^{\text{sort}}_{\text{vol\_min}}$ does not penalize extreme volume sizes, and that it takes minimum as well as maximum which, as functions of the data, are not as smooth as taking a summation. Throughout our experiments in the main text, we hence use the loss function $\mathcal{L}^{\text{sort}}_{\text{vol\_sum}}$.

B Implementation details

B.1 Code

To fully reproduce our results, anonymized code and preprocessed data are available at `https://anonymous.4open.science/r/1b728e97-cc2b-4e6a-98ea-37668813536c`.

B.2 Hardware

Experiments were conducted on a compute node with 8 Nvidia RTX 8000, 48 Intel Xeon Silver 4116 CPUs and 1000GB RAM, a compute node with 4 NVIDIA GeForce RTX 2080, 32 Intel Xeon E5-2690 v3 CPUs and 64GB RAM, a compute node with 2 NVIDIA Tesla K80, 16 Intel Xeon

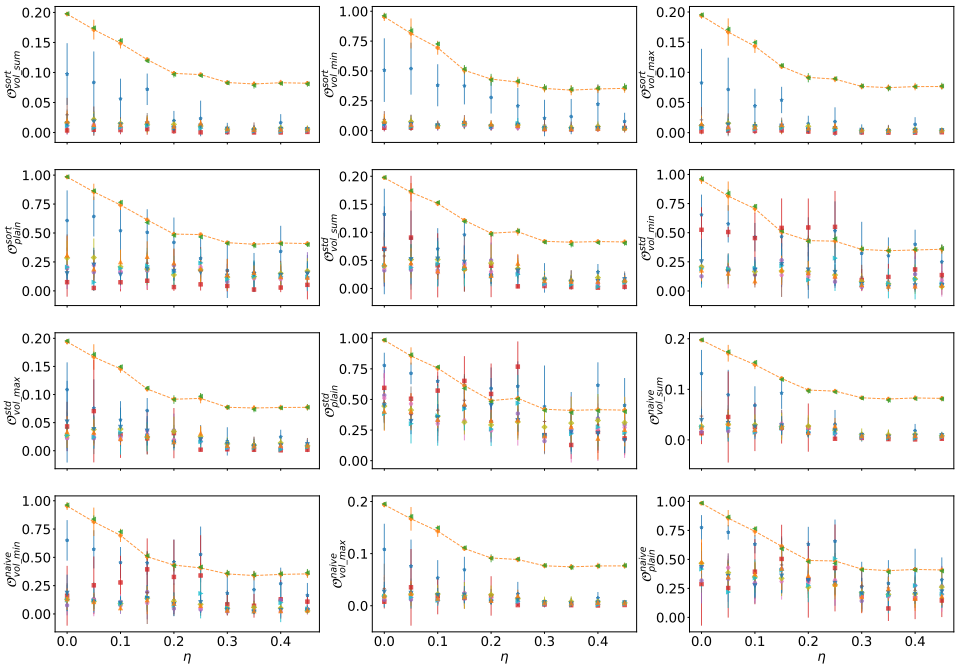

Figure 6: Imbalance scores comparison of loss functions on DSBM with 1000 nodes, 5 blocks, $\rho = 1, p = 0.02$ without ambient nodes, of the **complete meta-graph** structure. The legend is the same as Figure 5(a).

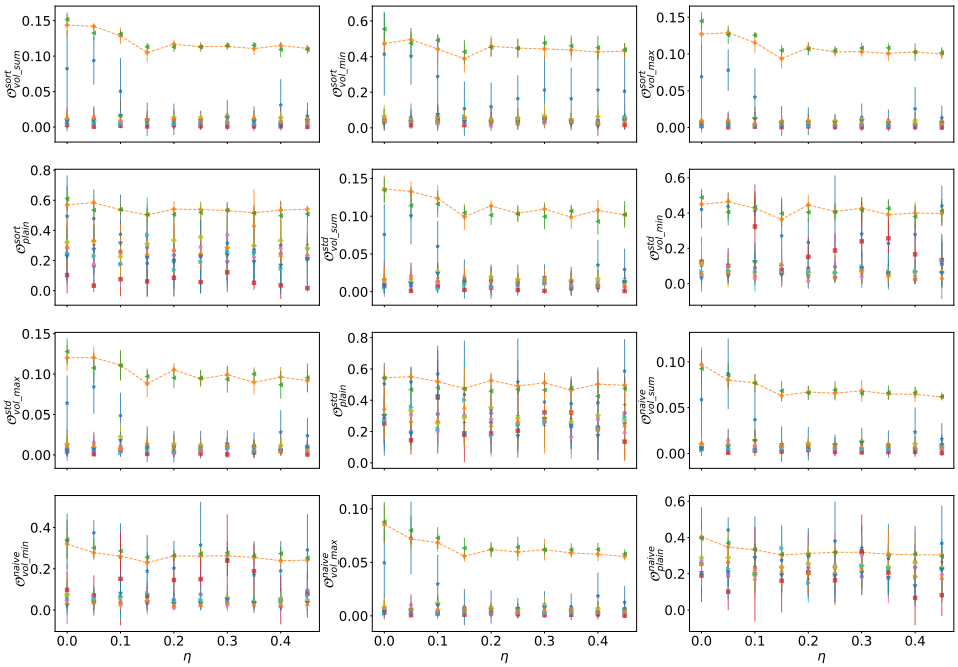

Figure 7: Imbalance scores comparison of loss functions on DSBM with 1000 nodes, 5 blocks, $\rho = 1, p = 0.02$ without ambient nodes, of the **cyclic meta-graph** structure. The legend is the same as Figure 5(a).

E5-2690 CPUs and 252GB RAM, and an Intel 2.90GHz i7-10700 processor with 8 cores and 16 threads.

With this setup, all experiments for spectral methods, MagNet, DiGCN and DIGRAC can be completed within two days, including repeated experiments, to obtain averages over multiple runs. DGCN and DiGCN_ib have much longer run time (especially DGCN, which is space-consuming, and we cannot run many experiments in parallel), with a total of three days for both of them to finish.

B.3 Data

The results comparing DIGRAC with other methods on synthetic data are averaged over 50 runs, five synthetic networks under the same setting, each with 10 different data splits. For synthetic data, 10% of all nodes are selected as test nodes for each cluster (the actual number is the ceiling of the total number of nodes times 0.1, to avoid falling below 10% of test nodes), 10% are selected as validation nodes (for model selection and early-stopping; again, we consider the ceiling for the actual number), while the remaining roughly 80% are selected as training nodes (the actual number can never be higher than 80% due to using the ceiling for both the test and validation splits).

For real-world data sets, we extract the largest weakly connected component for experiments, as our framework could be applied to different weakly connected components, if the digraph is disconnected. When "ground-truth" is given, test results are averaged over 10 different data splits on one network. When no labels are available, results are averaged over 10 different data splits.

Averaged results are reported with error bars representing one standard deviation in the figures, and plus/minus one standard deviation in the tables.

For real-world data sets, we choose the number K of clusters in the meta-graph and the number β of edges between clusters in the meta-graph as follows. As they are needed as input for DIGRAC, we resort to Herm_rw [12] as an initial view of the network clustering. When a suitable meta-graph is suggested in a previous publication, then we use that choice. Otherwise, the number K of clusters is determined using the clustering from Herm_rw. First, we pick a range of K, and for each K, we calculate the global imbalance scores and plot the predicted meta-graph flow matrix $\mathbf{F}'$ based on the clustering from Herm_rw. Its entries are defined as

$$\mathbf{F}'(k,l) = \mathbb{1}(W(\mathcal{C}_k,\mathcal{C}_l) + W(\mathcal{C}_l,\mathcal{C}_k) > 0) \times \frac{W(\mathcal{C}_k,\mathcal{C}_l)}{W(\mathcal{C}_k,\mathcal{C}_l) + W(\mathcal{C}_l,\mathcal{C}_k)}. \tag{12}$$

These entries can be viewed as predicted probabilities of edge directions. Then, we choose K from this range so that the predicted meta-graph flow matrix has the highest imbalance scores and strong imbalance in the predicted meta-graph flow matrix.

The choice of β is as follows. We plot the ranked pairs of CI^{plain} values from Herm_rw and select the β which is at least as large as $K-2$, to allow the meta-graph to be connected, and which corresponds to a large drop in the plot. Figures 14 (d) and 15 (d), respectively, give two examples.

When "ground-truth" labels are provided, as for example for *Cora-ML* and *CiteSeer*, we plot the ranked pairs of CI^{plain} values based on the labels, as for example provided in Figures 8. In these examples, with $K = 7$ ($K = 6$, respectively), we choose $\beta = 11$ ($\beta = 9$, respectively) for *Cora-ML* (*CiteSeer*, respectively).

Here we provide a brief description for each of the data sets; Table 4 gives the number, n, of nodes, the number, $|\mathcal{E}|$, of directed edges, the number $|\mathcal{E}^r|$, of reciprocal edges (self-loops are counted once and for $u \neq v$, a reciprocal edge $u \to v, v \to u$ is counted twice) as well as their percentage among all edges, for the real-world networks, illustrating the variability in network size and density (defined as $|\mathcal{E}|/[n(n-1)]$).

• *Telegram* [5] is a pairwise influence network between $n = 245$ Telegram channels with $|\mathcal{E}| = 8,912$ directed edges. It is found in [5] that this network reveals a core-periphery structure in the sense of [15]. Following [5] we assume $K = 4$ clusters, and the core-periphery structures gives $\beta = 5$.

• *Blog* [1] records $|\mathcal{E}| = 19,024$ directed edges between $n = 1,212$ political blogs from the 2004 US presidential election. In [1] it is found that there is an underlying structure with $K = 2$ clusters corresponding to the Republican and Democratic parties. Hence we choose $K = 2$ and $\beta = 1$.

• *Migration* [36] reports the number of people that migrated between pairs of counties in the US during 1995-2000. It involves $n = 3,075$ countries and $|\mathcal{E}| = 721,432$ directed edges after obtaining

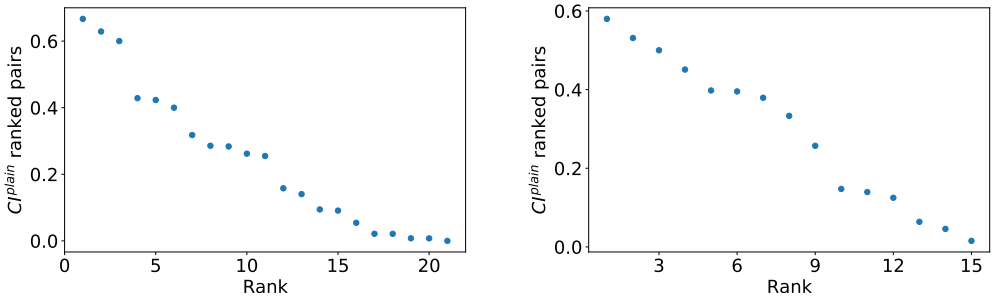

(a) *Cora-ML*. (b) *CiteSeer*.

Figure 8: Ranked pairs of CI^{plain} values based on the labels of *Cora-ML* and *CiteSeer*. We choose $\beta = 11$ for *Cora-ML* and $\beta = 0$ for *CiteSeer*.

the largest weakly connected component. We choose $K = 10$ and $\beta = 9$, following [12].
• *WikiTalk* [27] contains all users and discussion from the inception of Wikipedia until Jan. 2008. The $n = 2,388,953$ nodes in the network represent Wikipedia users and a directed edge from node v_i to node v_j denotes that user i edited at least once a talk page of user j. There are $|\mathcal{E}| = 5,018,445$ edges. We choose $K = 10$ clusters among candidates $\{2, 3, 5, 6, 8, 10\}$, and $\beta = 10$.
• *Cora-ML* and *CiteSeer* are citation networks [4] with class labels (7 and 6 classes, respectively). Inspecting Figures 8, we use $\beta = 11$ and $\beta = 9$, respectively.

Table 4: Summary statistics for the real-world networks.

data set	n	$\lvert\mathcal{E}\rvert$	density	weighted	$\lvert\mathcal{E}^r\rvert$	$\frac{\lvert\mathcal{E}^r\rvert}{\lvert\mathcal{E}\rvert}(\%)$
Telegram	245	8,912	$1.28 \cdot 10^{-2}$	True	1,572	17.64
Blog	1,222	19,024	$1.49 \cdot 10^{-1}$	True	4,617	24.27
Migration	3,075	721,432	$7.63 \cdot 10^{-2}$	True	351,100	48.67
WikiTalk	2,388,953	5,018,445	$8.79 \cdot 10^{-7}$	False	723,526	14.42
Cora-ML	2995	8416	$9.39 \cdot 10^{-4}$	False	516	6.13
CiteSeer	3312	4715	$4.30e \cdot 10^{-4}$	False	234	4.96

As input features, after obtaining eigenvectors from Hermitian matrices constructed as in [12], we standardize each column vector so that it has mean zero and variance one. We use these features for all GNN methods except MagNet, since MagNet has its own way of generating random features of dimension one.

B.4 Hyperparameters

We conduct hyperparmeter selection via a greedy search. To explain the details, consider for example the following synthetic data setting: DSBM with 1000 nodes, 5 clusters, $\rho = 1$, and $p = 0.02$, without ambient nodes under different hyperparameter settings. By default, we use the loss function $\mathcal{L}^{\text{sort}}_{\text{vol\_sum}}$, $d = 32$ hidden units, hop $h = 2$, and no seed nodes. Instead of a grid search, we tune hyperparameters according to what performs the best in the default setting of the respective GNN method. The procedure starts with a random setting. For the next iteration, the hyperparameters are set to the current best setting (based on the last iteration), independently. For example, if we start with $a = 1, b = 2, c = 3$, and we find that under this default setting, the best a (when fixing $b = 2, c = 3$) is 2 and the best b (when fixing $a = 1, c = 3$) is 3, and the best c is 3 (when fixing $a = 1, b = 2$), then for the next iteration, we set $a = 2, b = 3, c = 3$. If two settings give similar results, we choose the simpler setting, for example, the smaller hop size. When we reach a local optimum, we stop searching. Indeed, just a few iterations (less than five) were required for us to find the current setting, as DIGRAC tends to be robust to most hyperparameters.

Figure 9, 10 and 11 are plots corresponding to the same setting but for three different meta-graph structures, namely the complete meta-graph structure, the cycle structure but with ambient nodes, and the complete structure with ambient nodes, respectively.

In theory, more hidden units give better expressive power. To reduce complexity, we use 32 hidden units throughout, which seems to have desirable performance. We observe that for low-noise regimes, more hidden units actually hurt performance. We can draw a similar conclusion about the hyperparameter selection. In terms of τ, DIGRAC seems to be robust to different choices. Therefore, we use $\tau = 0.5$ throughout.

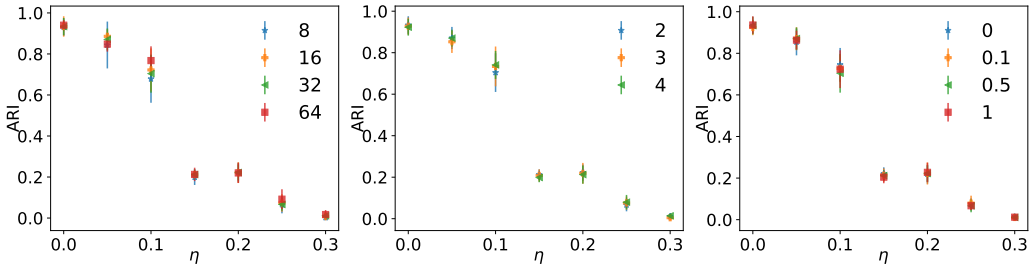

(a) Vary d. (b) Vary the hop h. (c) Vary τ.

Figure 9: Hyperparameter analysis on different hyperparameter settings on the **complete** DSBM with 1000 nodes, 5 clusters, $\rho = 1$, and $p = 0.02$ **without** ambient nodes.

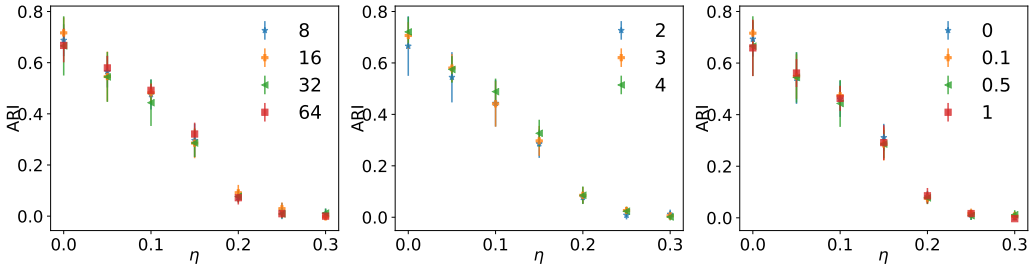

(a) Vary d. (b) Vary the hop h. (c) Vary τ.

Figure 10: Hyperparameter analysis on different hyperparameter settings on the **complete** DSBM with 1000 nodes, 5 clusters, $\rho = 1$, and $p = 0.02$ **with** ambient nodes.

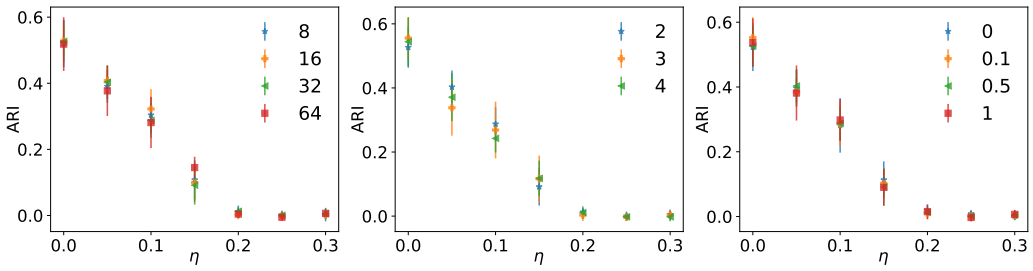

(a) Vary d. (b) Vary the hop h. (c) Vary τ.

Figure 11: Hyperparameter analysis on different hyperparameter settings on the **cycle** DSBM with 1000 nodes, 5 clusters, $\rho = 1$, and $p = 0.02$ **with** ambient nodes.

B.5 Use of seed nodes in a semi-supervised manner

B.5.1 Supervised loss

For seed nodes in $\mathcal{V}^{\text{seed}}$, similar to the loss function in [41], we use as a supervised loss function the sum of a cross-entropy loss and a triplet loss. The cross-entropy loss is given by

$$\mathcal{L}_{\text{CE}} = -\frac{1}{|\mathcal{V}^{\text{seed}}|} \sum_{v_i \in \mathcal{V}^{\text{seed}}} \sum_{k=1}^{K} \mathbb{1}(v_i \in \mathcal{C}_k) \log\left((\mathbf{p}_i)_k\right), \tag{13}$$

where $\mathbb{1}$ is the indicator function, $\mathcal{C}_k$ denotes the k^{th} cluster, and $(\mathbf{p}_i)_k$ denotes the k^{th} entry of probability vector $(\mathbf{p}_i)$. With the function $L : \mathbb{R}^2 \to \mathbb{R}$ given by $L(x, y) = [x - y]_+$ (where the subscript $+$ indicates taking the maximum of the expression value and 0), the triplet loss is defined as

$$\mathcal{L}_{\text{triplet}} = \frac{1}{|\mathcal{S}|} \sum_{(v_i, v_j, v_k) \in \mathcal{S}} L(\text{CS}(\mathbf{z}_i, \mathbf{z}_j), \text{CS}(\mathbf{z}_i, \mathbf{z}_k), \tag{14}$$

where $\mathcal{S} \subseteq \mathcal{V}^{\text{seed}} \times \mathcal{V}^{\text{seed}} \times \mathcal{V}^{\text{seed}}$ is a set of node triplets: v_i is an anchor seed node, and v_j is a seed node from the same cluster as the anchor, while v_k is from a different cluster; and $\text{CS}(\mathbf{z}_i, \mathbf{z}_j)$ is the cosine similarity of the embeddings of nodes v_i and v_j. We choose cosine similarity so as to avoid sensitivity to the magnitude of the embeddings. The triplet loss is designed so that, given two seed nodes from the same cluster and one seed node from a different cluster, the respective embeddings of the pairs from different clusters should be farther away than the embedding of the pair within the same cluster.

We then consider the weighted sum $\mathcal{L}_{\text{CE}} + \gamma_t \mathcal{L}_{\text{triplet}}$ as the supervised part of the loss function for DIGRAC, for some parameter $\gamma_t > 0$. The parameter γ_t arises as follows. The cosine similarity between two randomly picked vectors in d dimensions is bounded by $\sqrt{\ln(d)/d}$ with high probability. In our experiments $d = 32$, and $\sqrt{\ln(2d)/(2d)} \approx 0.25$. In contrast, for fairly uniform clustering, the cross-entropy loss grows like $\log n$, which in our experiments ranges between 3 and 17. Thus some balancing of the contribution is required. Following [41], we choose $\gamma_t = 0.1$ in our experiments.

B.5.2 Overall objective function

By combining Eq. (13), Eq. (14), and Eq. (4), our objective function for semi-supervised training with known seed nodes minimizes

$$\mathcal{L} = \mathcal{L}^{\text{sort}}_{\text{vol\_sum}} + \gamma_s(\mathcal{L}_{\text{CE}} + \gamma_t \mathcal{L}_{\text{triplet}}), \tag{15}$$

where $\gamma_s, \gamma_t > 0$ are weights for the supervised part of the loss and triplet loss within the supervised part, respectively. We set $\gamma_s = 50$ as we want our model to perform well on seed nodes. The weights could be tuned depending on how important each term is perceived to be.

B.6 Training

For all synthetic data, we train DIGRAC with a maximum of 1000 epochs, and stop training when no gain in validation performance is achieved for 200 epochs (early-stopping). For real-world data, no "ground-truth" labels are available; we use all nodes to train and stop training when the training loss does not decrease for 200 epochs, or when we reach the maximum number of epochs, 1000.

For the two-layer MLP, we do not have a bias term for each layer, and we use Rectified Linear Unit (ReLU) followed by a dropout layer with 0.5 dropout probability between the two layers, following [41]. We use Adam [23] as the optimizer and ℓ_2 regularization with weight decay $5 \cdot 10^{-4}$ to avoid overfitting. We use as learning rate 0.01 throughout.

B.7 Implementation details for the comparison methods

In our experiments, we compare DIGRAC against five spectral methods and five GNN-based supervised methods on synthetic data, and spectral methods on real data. The reason we are not able to compare DIGRAC with the above GNNs on these data sets is due to the fact that these data sets do not have labels, which are required by the other GNN methods. We use the same hyperparameter settings stated in these papers. Data splits for all models are the same; the comparison GNNs are trained with 80% nodes under label supervision.

For MagNet, we use $q = 0.25$ for the phase matrix as in [45], where $q = 0.25$ was used for two out of their three synthetic data sets, and $q = 0.1$ for their third data set. Code for MagNet, with a sparse implementation, is included in our anonymized repository, with the original version from `https://github.com/matthew-hirn/magnet`. We use the code from `https://github.com/flyingtango/DiGCN/blob/main/code/digcn.py` to obtain the log of probability matrix $\mathbf{P}$ for the methods DiGCN and DiGCN_app. The only difference between these two methods is whether or not to use approximate Laplacian based on personalized PageRank. The "adj_type" options for them correspond to "or" and "appr", respectively.

For DiGCN_ib, we use the code from `https://github.com/flyingtango/DiGCN/blob/main/code/digcn_ib.py` with option "adj_type" equals "ib". As a recommended option in [42], we use three layers for DiGCN_ib and two layers for DiGCN and DiGCN_app. All other settings are the same as in the original paper [42].

B.8 Complexity analysis

To avoid computationally expensive and space unfriendly matrix operations, as described in Eq. (1), DIGRAC uses an efficient sparsity-aware implementation, described in Algorithm 1 in the main text, without explicitly calculating the sets of powers $\mathcal{A}^{s,h}$ and $\mathcal{A}^{t,h}$. The algorithm also takes sparse matrices as input, and never explicitly computes a multiplication of two $n \times n$ matrices. Therefore, for input feature dimension and hidden dimension $d \ll n$, time and space complexity of DIMPA (and implicitly of DIGRAC) is $\mathcal{O}(|\mathcal{E}|dh + 2ndK)$ and $\mathcal{O}(2|\mathcal{E}| + 4nd + nK)$, respectively [20, 18]. For large-scale networks, DIMPA is amenable to a minibatch version using neighborhood sampling, similar to the minibatch forward propagation algorithm in [19, 31].

C More results on synthetic data

C.1 An additional meta-graph structure

Recall that the Directed Stochastic Block Models used in our experiments depend on a meta-graph adjacency matrix $\mathbf{F}$ and a filled version of it, $\tilde{\mathbf{F}}$, for some number of clusters, K, and noise level $\eta \leq 0.5$. The meta-graph adjacency matrix $\mathbf{F}$ is generated from some meta-graph structure, called $\mathcal{M}$. Based on $\mathcal{M}$, the filled meta-graph $\tilde{\mathbf{F}}$ replaces every zero in $\mathbf{F}$ that is not part of the imbalance structure with 0.5, independently of the choice of η. It is the filled meta-graph $\tilde{\mathbf{F}}$ which we feed into the DSBM generation process.The filled meta-graph creates a number of *ambient nodes* which correspond to entries which are not part of the imbalance structure and thus are not part of a meaningful cluster; the set of *ambient nodes* is also called the *ambient cluster*.

Here, we introduce an additional meta-graph structure, called "multipartite", following [16]. First, when there are no ambient nodes: we divide the index set into three sets; setting $i_1 = \lfloor \frac{K}{9} \rfloor, i_2 = \lfloor \frac{3K}{9} \rfloor + i_1$, let

$$\begin{aligned} \mathbf{F}_{k,l} &= (1-\eta)\mathbb{1}(k < i_1, i_1 \leq l < i_2) + \eta\mathbb{1}(i_1 \leq k < i_2, l \geq i_2) \\ &\quad +(1-\eta)\mathbb{1}(k \geq i_2, i_1 \leq l < i_2) + \eta\mathbb{1}(i_1 \leq k < i_2, l < i_1). \end{aligned}$$

When we have ambient nodes, the construction involves two steps, with the first step the same as the above but with the following changes: divide the indices into three sets, with set boundaries given by $i_1 = \lfloor \frac{K-1}{9} \rfloor, i_2 = \lfloor \frac{3(K-1)}{9} \rfloor + i_1$. The second step is to assign 0 (respectively, 0.5) to the last row and the last column of $\mathbf{F}$ (respectively, $\tilde{\mathbf{F}}$).

C.2 Additional comparison plots and analysis

Figure 12 compares the numerical performance of DIGRAC with other methods on four more settings of synthetic data, namely, a cycle structure with three clusters, a complete structure with ten clusters, a multipartite structure with ten clusters, and a star structure with five clusters. Considering the results in Section 5 and Figure 12, we remark that DIGRAC gives state-of-the-art results on a wide range of network densities and noise levels, on different scales of the networks, and with different meta-graph structures, whether or not ambient nodes exist.

Note that the multipartite, the cycle and the star settings correspond to the intuition behind [42] which assumes that nodes are similar if their set of k^{th}-order neighbourhoods are similar; here the second-order neighbourhoods are similar by design. For networks with underlying meta-graph structure "star", "cycle" or "multipartite", clusters could be determined by grouping nodes that share similar in-neighbors and out-neighbors together, which aligns well with the second-order proximity used in DGCN and DiGCN_ib from [43]. Therefore, these methods are naturally well-suited for dealing with the such synthetic data. We also note that although DIGRAC does not explicitly use second-order proximity, it can achieve comparable performance with DGCN and DiGCN_ib. This indicates DIGRAC's flexibility to adapt to directed networks with different underlying topologies,

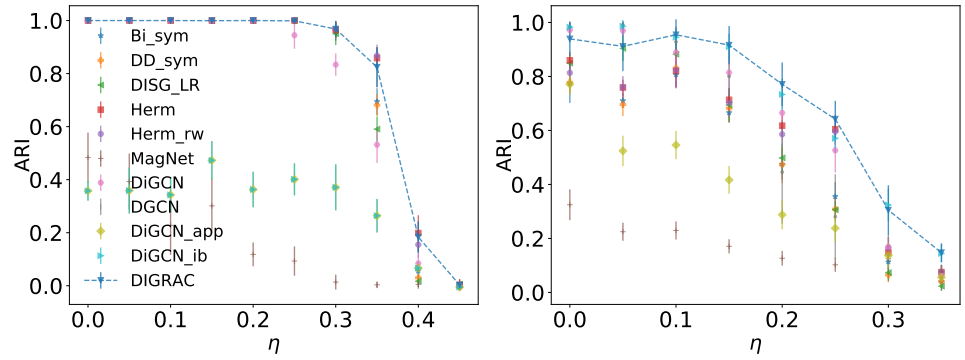

(a) DSBM("cycle", F, $n = 1000, K = 3, p = 0.1, \rho = 1$)

(b) DSBM("complete", T, $n = 1000, K = 10, p = 0.1, \rho = 1$)

(c) DSBM("multipartite", T, $n = 1000, K = 10, p = 0.1, \rho = 1$)

(d) DSBM("star", F, $n = 5000, K = 5, p = 0.02, \rho = 1$)

Figure 12: Node clustering test ARI comparison on four additional synthetic data sets. Dashed lines highlight DIGRAC's performance. Error bars are given by one standard error. Abbreviations for all the methods are given in Section 4 in the main text.

without explicitly utilizing higher-order proximity. On the other hand, DiGCN_ib is fully supervised, and takes much more space and time to implement, than DIGRAC. This is partially due to the use of the so-called *inception blocks* in DiGCN_ib, where multi-scale directed structure features are encoded and fused with a fusion function. As stated in [42], the worst space complexity is $\mathcal{O}(k'n^2)$, where k' is the order of proximity to consider (we use $k' = 2$ throughout). The eigenvalue decomposition in the preprocessing step is $\mathcal{O}(n^3)$. We also remark that the approximate Laplacian based on personalized PageRank, when no inception blocks are used, performs no better than the simpler implementation without the approximation. We conclude that overall DIGRAC is a fast method for general directed clustering when directionality is the main signal, which performs as well as custom-tailored methods when the proximity neighborhood heuristic holds, while outperforming all tested methods on the complete meta-graph, where the proximity neighborhood heuristic does not hold.

D Additional results on real-world data

D.1 Extended result tables

Tables 5, 6, 7 and 8 provide a detailed comparison of DIGRAC with spectral methods. Since no labeling information is available and all of the other competing GNN methods require labels, we do not compare DIGRAC with them on these real data sets.

In Tables 5, 6, 7 and 8, we report 12 combinations of global imbalance scores by data set. The naming convention of these imbalance scores is provided in Table 3. To assess how balanced our recovered clusters are in terms of sizes, we also report the size ratio, which is defined as the size of the largest predicted cluster to the smallest one, and the standard deviation of sizes, size std, in order to show

how varied the sizes of predicted clusters are. For a relatively balanced clustering, we expect the latter two terms to be small.

Table 5: Performance comparison on *Telegram*. The best is marked in **bold red** and the second best is marked in underline blue.

Metric/Method	Bi_sym	DD_sym	DISG_LR	Herm	Herm_rw	DIGRAC
$\mathcal{O}^{\text{sort}}_{\text{vol\_sum}}$	0.21±0.00	0.21±0.00	0.21±0.01	0.20±0.01	0.14±0.00	**0.32±0.01**
$\mathcal{O}^{\text{sort}}_{\text{vol\_min}}$	0.67±0.00	0.61±0.00	0.66±0.02	0.66±0.02	0.19±0.00	**0.79±0.06**
$\mathcal{O}^{\text{sort}}_{\text{vol\_max}}$	0.20±0.00	0.20±0.00	0.20±0.01	0.19±0.01	0.12±0.00	**0.29±0.01**
$\mathcal{O}^{\text{sort}}_{\text{plain}}$	0.80±0.00	0.75±0.00	0.78±0.03	0.76±0.04	0.59±0.00	**0.96±0.01**
$\mathcal{O}^{\text{std}}_{\text{vol\_sum}}$	0.26±0.00	0.26±0.00	0.26±0.01	0.25±0.02	**0.35±0.00**	0.28±0.01
$\mathcal{O}^{\text{std}}_{\text{vol\_min}}$	**0.84±0.00**	0.76±0.00	0.82±0.03	0.82±0.03	0.49±0.00	0.73±0.03
$\mathcal{O}^{\text{std}}_{\text{vol\_max}}$	0.25±0.00	0.25±0.00	0.25±0.01	0.24±0.02	**0.29±0.00**	0.25±0.01
$\mathcal{O}^{\text{std}}_{\text{plain}}$	**1.00±0.00**	0.94±0.00	0.98±0.04	0.95±0.04	0.99±0.00	0.90±0.05
$\mathcal{O}^{\text{naive}}_{\text{vol\_sum}}$	0.26±0.00	0.26±0.00	0.26±0.01	0.25±0.02	0.23±0.00	**0.27±0.01**
$\mathcal{O}^{\text{naive}}_{\text{vol\_min}}$	**0.84±0.00**	0.76±0.00	0.82±0.03	0.82±0.03	0.32±0.00	0.72±0.04
$\mathcal{O}^{\text{naive}}_{\text{vol\_max}}$	**0.25±0.00**	**0.25±0.00**	**0.25±0.01**	0.24±0.02	0.20±0.00	0.24±0.01
$\mathcal{O}^{\text{naive}}_{\text{plain}}$	**1.00±0.00**	0.94±0.00	0.98±0.04	0.95±0.04	0.99±0.00	0.89±0.06
size ratio	242	242.00	242.00	242.00	53.00	**3.09**
size std	104.36	104.36	104.36	104.36	63.46	**26.39**

Table 6: Performance comparison on *Blog*. The best is marked in **bold red** and the second best is marked in underline blue.

Metric/Method	Bi_sym	DD_sym	DISG_LR	Herm	Herm_rw	DIGRAC
$\mathcal{O}^{\text{sort}}_{\text{vol\_sum}}$	0.07±0.00	0.00±0.00	0.05±0.00	0.37±0.00	0.00±0.00	**0.44±0.00**
$\mathcal{O}^{\text{sort}}_{\text{vol\_min}}$	0.33±0.00	0.05±0.00	0.31±0.00	0.78±0.01	**0.89±0.00**	0.76±0.00
$\mathcal{O}^{\text{sort}}_{\text{vol\_max}}$	0.05±0.00	0.00±0.00	0.04±0.00	0.26±0.00	0.00±0.00	**0.40±0.00**
$\mathcal{O}^{\text{sort}}_{\text{plain}}$	0.33±0.00	0.05±0.00	0.31±0.00	0.78±0.01	**0.89±0.00**	0.76±0.00
$\mathcal{O}^{\text{std}}_{\text{vol\_sum}}$	0.07±0.00	0.00±0.00	0.05±0.00	0.37±0.00	0.00±0.00	**0.44±0.00**
$\mathcal{O}^{\text{std}}_{\text{vol\_min}}$	0.33±0.00	0.05±0.00	0.31±0.00	0.78±0.01	**0.89±0.00**	0.76±0.00
$\mathcal{O}^{\text{std}}_{\text{vol\_max}}$	0.05±0.00	0.00±0.00	0.04±0.00	0.26±0.00	0.00±0.00	**0.40±0.00**
$\mathcal{O}^{\text{std}}_{\text{plain}}$	0.33±0.00	0.05±0.00	0.31±0.00	0.78±0.01	**0.89±0.00**	0.76±0.00
$\mathcal{O}^{\text{naive}}_{\text{vol\_sum}}$	0.07±0.00	0.00±0.00	0.05±0.00	0.37±0.00	0.00±0.00	**0.44±0.00**
$\mathcal{O}^{\text{naive}}_{\text{vol\_min}}$	0.33±0.00	0.05±0.00	0.31±0.00	0.78±0.01	**0.89±0.00**	0.76±0.00
$\mathcal{O}^{\text{naive}}_{\text{vol\_max}}$	0.05±0.00	0.00±0.00	0.04±0.00	0.26±0.00	0.00±0.00	**0.40±0.00**
$\mathcal{O}^{\text{naive}}_{\text{plain}}$	0.33±0.00	0.05±0.00	0.31±0.00	0.78±0.01	**0.89±0.00**	0.76±0.00
size ratio	8.70	2.45	6.10	11.93	44.26	**1.86**
size std	485.00	256.20	439.00	516.50	584.00	**183.20**

Tables 5, 6, 7 and 8 reveal that DIGRAC provides competitive global imbalance scores in all of the 12 objectives introduced, and across all the real data sets, usually outperforming all the other methods. Note that Bi_sym and DD_sym are not able to generate results for *WikiTalk*, as large $n \times n$ matrix multiplication with its transpose causes memory issue, when $n = 2,388,953$. Small values of the size ratio and size standard deviation suggest that the normalization in the loss function penalizes tiny clusters, and that DIGRAC tends to predict balanced cluster sizes.

Table 7: Performance comparison on *Migration*. The best is marked in **bold red** and the second best is marked in underline blue.

Metric/Method	Bi_sym	DD_sym	DISG_LR	Herm	Herm_rw	DIGRAC
$\mathcal{O}^{\text{sort}}_{\text{vol\_sum}}$	0.03±0.00	0.01±0.00	0.01±0.00	**0.07±0.00**	0.01±0.00	0.04±0.00
$\mathcal{O}^{\text{sort}}_{\text{vol\_min}}$	0.20±0.01	0.12±0.02	0.14±0.00	**0.21±0.01**	0.05±0.02	0.18±0.02
$\mathcal{O}^{\text{sort}}_{\text{vol\_max}}$	0.03±0.00	0.01±0.00	0.01±0.00	**0.06±0.00**	0.00±0.00	0.04±0.00
$\mathcal{O}^{\text{sort}}_{\text{plain}}$	0.46±0.00	0.29±0.02	0.26±0.00	**0.62±0.02**	0.40±0.00	0.32±0.11
$\mathcal{O}^{\text{std}}_{\text{vol\_sum}}$	0.01±0.00	0.00±0.00	0.00±0.00	0.02±0.00	0.00±0.00	**0.03±0.01**
$\mathcal{O}^{\text{std}}_{\text{vol\_min}}$	0.09±0.00	0.04±0.01	0.05±0.00	0.08±0.01	0.02±0.01	**0.11±0.03**
$\mathcal{O}^{\text{std}}_{\text{vol\_max}}$	0.01±0.00	0.00±0.00	0.00±0.00	0.01±0.00	0.00±0.00	**0.02±0.01**
$\mathcal{O}^{\text{std}}_{\text{plain}}$	0.23±0.00	0.14±0.01	0.12±0.00	**0.32±0.01**	0.25±0.01	0.21±0.03
$\mathcal{O}^{\text{naive}}_{\text{vol\_sum}}$	0.01±0.00	0.00±0.00	0.00±0.00	0.02±0.00	0.00±0.00	**0.03±0.01**
$\mathcal{O}^{\text{naive}}_{\text{vol\_min}}$	0.08±0.00	0.04±0.01	0.05±0.00	0.08±0.01	0.02±0.01	**0.11±0.04**
$\mathcal{O}^{\text{naive}}_{\text{vol\_max}}$	0.01±0.00	0.00±0.00	0.00±0.00	0.01±0.00	0.00±0.00	**0.02±0.01**
$\mathcal{O}^{\text{naive}}_{\text{plain}}$	0.22±0.00	0.13±0.01	0.11±0.00	**0.31±0.01**	0.22±0.00	0.21±0.03
size ratio	3043.80	722.62	**25.78**	3059.20	415.88	203.23
size std	912.10	861.28	409.90	917.23	844.75	**342.38**

Table 8: Performance comparison on *WikiTalk*. The best is marked in **bold red** and the second best is marked in underline blue.

Metric/Method	DISG_LR	Herm	Herm_rw	DIGRAC
$\mathcal{O}^{\text{sort}}_{\text{vol\_sum}}$	0.18±0.03	0.15±0.02	0.00±0.00	**0.24±0.05**
$\mathcal{O}^{\text{sort}}_{\text{vol\_min}}$	0.10±0.03	0.22±0.05	0.26±0.00	**0.28±0.13**
$\mathcal{O}^{\text{sort}}_{\text{vol\_max}}$	0.16±0.03	0.09±0.01	0.00±0.00	**0.19±0.04**
$\mathcal{O}^{\text{sort}}_{\text{plain}}$	0.87±0.08	0.99±0.01	0.98±0.00	**1.00±0.00**
$\mathcal{O}^{\text{std}}_{\text{vol\_sum}}$	**0.17±0.04**	0.06±0.01	0.01±0.00	0.14±0.02
$\mathcal{O}^{\text{std}}_{\text{vol\_min}}$	0.09±0.02	0.09±0.02	**0.27±0.00**	0.18±0.08
$\mathcal{O}^{\text{std}}_{\text{vol\_max}}$	**0.15±0.04**	0.04±0.00	0.00±0.00	0.11±0.02
$\mathcal{O}^{\text{std}}_{\text{plain}}$	0.72±0.03	0.70±0.05	**0.98±0.00**	0.84±0.06
$\mathcal{O}^{\text{naive}}_{\text{vol\_sum}}$	0.10±0.02	0.04±0.00	0.00±0.00	**0.12±0.01**
$\mathcal{O}^{\text{naive}}_{\text{vol\_min}}$	0.06±0.03	0.07±0.02	**0.26±0.00**	0.15±0.07
$\mathcal{O}^{\text{naive}}_{\text{vol\_max}}$	**0.09±0.02**	0.03±0.00	0.00±0.00	**0.09±0.01**
$\mathcal{O}^{\text{naive}}_{\text{plain}}$	0.64±0.04	0.61±0.04	**0.98±0.00**	0.76±0.06
size ratio	1190162.25	2217434.50	**250.48**	71765.14
size std	713813.72	660060.33	657941.88	**643220.37**

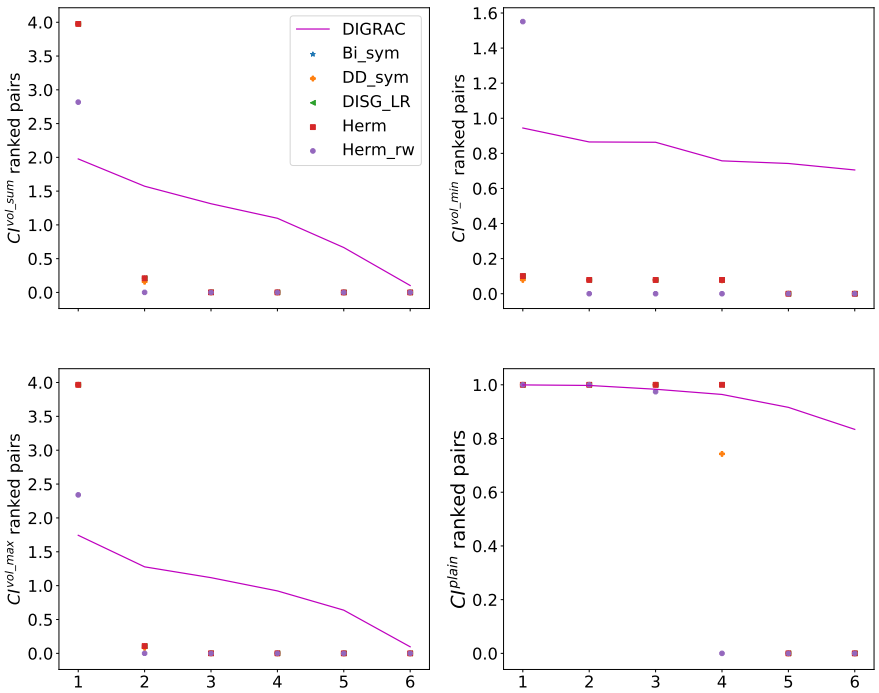

Figure 13: Ranked pairs of pairwise imbalance recovered by comparing methods for different choices of normalization on the *Telegram* data set. Lines are used to highlight DIGRAC's performance.

D.2 Ranked pairwise imbalance scores

We also plot the ranked pairwise imbalance scores for all data sets except *Blog*, which has only one possible pairwise imbalance score. Figures 13, 14 and 15 illustrate that DIGRAC is able to provide comparable or higher pairwise imbalance scores for the leading pairs, especially on $\mathrm{CI}^{\mathbf{vol\_min}}$ pairs. We also observe that except for $\mathrm{CI}^{\mathbf{plain}}$, DIGRAC has a less rapid drop in pairwise imbalance scores after the first leading pair compared to Herm and Herm_rw, which can have a few pairs with higher imbalance scores than DIGRAC.

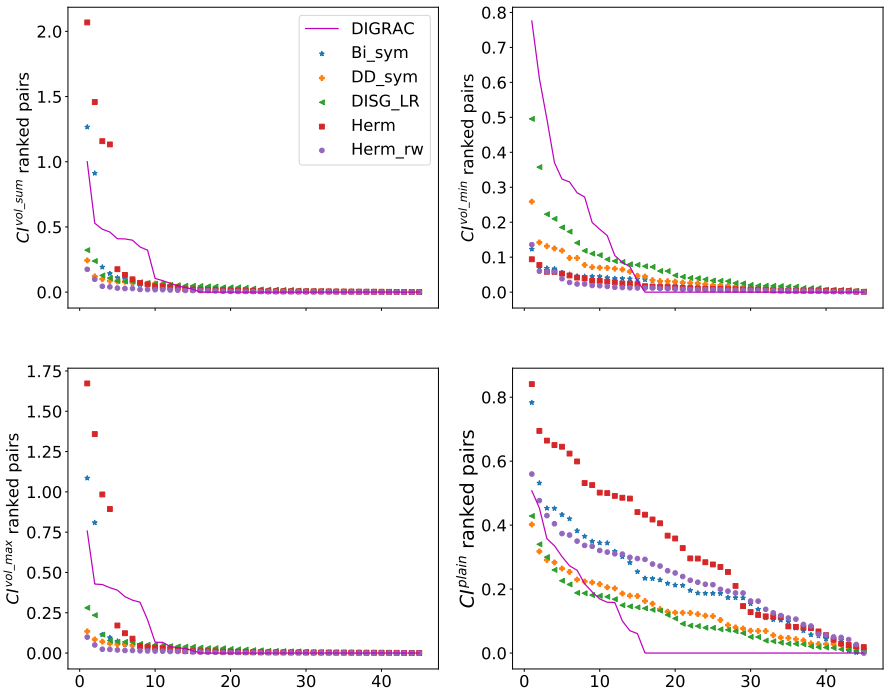

Figure 14: Ranked pairs of pairwise imbalance recovered by comparing methods for different choices of normalization on the *Migration* data set. Lines are used to highlight DIGRAC's performance.

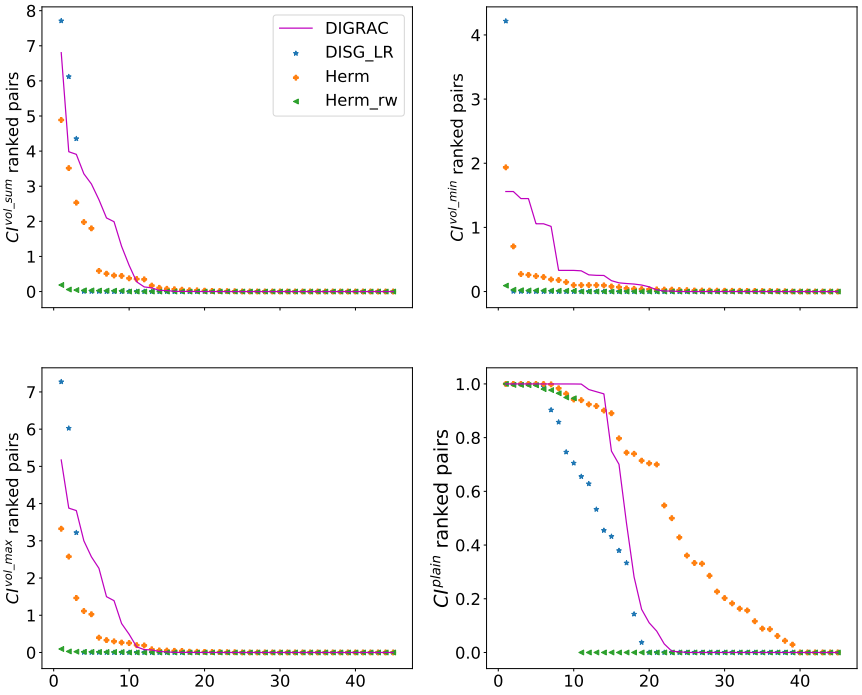

Figure 15: Ranked pairs of pairwise imbalance recovered by comparing methods for different choices of normalization on *WikiTalk* data set. Lines are used to highlight DIGRAC's performance.

D.3 Predicted meta-graph flow matrix plots

For each data set, we plot the predicted meta-graph flow matrix $\mathbf{F}'$ defined in Eq. (12).

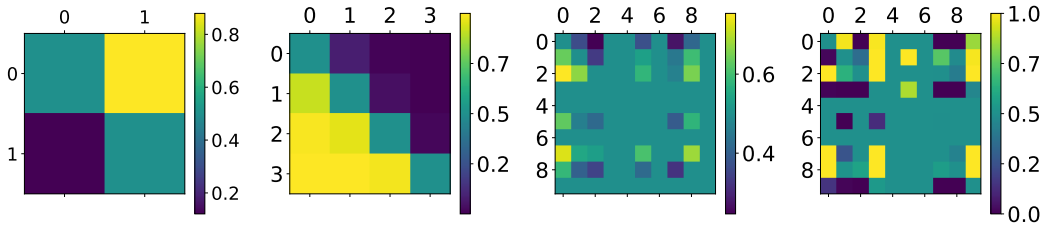

(a) *Blog* (b) *Telegram* (c) *Migration* (d) *WikiTalk*

Figure 16: Predicted meta-graph flow matrix from DIGRAC of four real-world data sets.

From Figure 16, we conclude that DIGRAC is able to recover a directed flow imbalance between clusters in all of the selected data sets. Figure 16a shows a clear cut imbalance between two clusters, possibly corresponding to the Republican and Democratic parties. Figure 16b plots imbalance flows in the real data set *Telegram*, where cluster 3 is a core-transient cluster, cluster 0 is a core-sink cluster, cluster 2 is a periphery-upstream cluster, while cluster 1 is a periphery-downstream cluster [15, 5]. For *WikiTalk*, illustrated in Figure 16d, the lower-triangular part entries are typically source nodes for edges, while the upper-triangular part are target nodes.

We also note that DIGRAC would not necessarily predict the same number of clusters as assumed, so that we do not need to specify the exact number of clusters before training DIGRAC; specifying the maximum number of possible clusters suffices.

D.4 Migration plots

We compare DIGRAC to five spectral methods for recovering clusters for the US migration data set, and plot the recovered clusters on a map. Note that all methods, except DIGRAC, recover either clusters which are trivially small in size or contain one very large dominant cluster (as in (a), (b) (d) and to some extent, also (e)). The DISG_LR clustering provides clear geographic boundaries, but was not able to recover the imbalance among clusters. Other spectral methods generally have a dominant cluster containing most of the nodes, whereas DIGRAC has more balanced cluster sizes.

When employing methods that symmetrize the adjacency matrix (as in (a) and (b)), the migration flows between counties in different states will be lost in the process. Furthermore, the visualization in Figure (c) shows that clusters align particularly well with the political and administrative boundaries of the US states, as previously observed in [11]. This outcome is not deemed too insightful, as it trivially reveals the fact there there is significant intra-state and inter-state migration, and does not uncover any of the information on latent migration patterns between far-away states, and more generally, between regions which are not necessarily geographically cohesive.

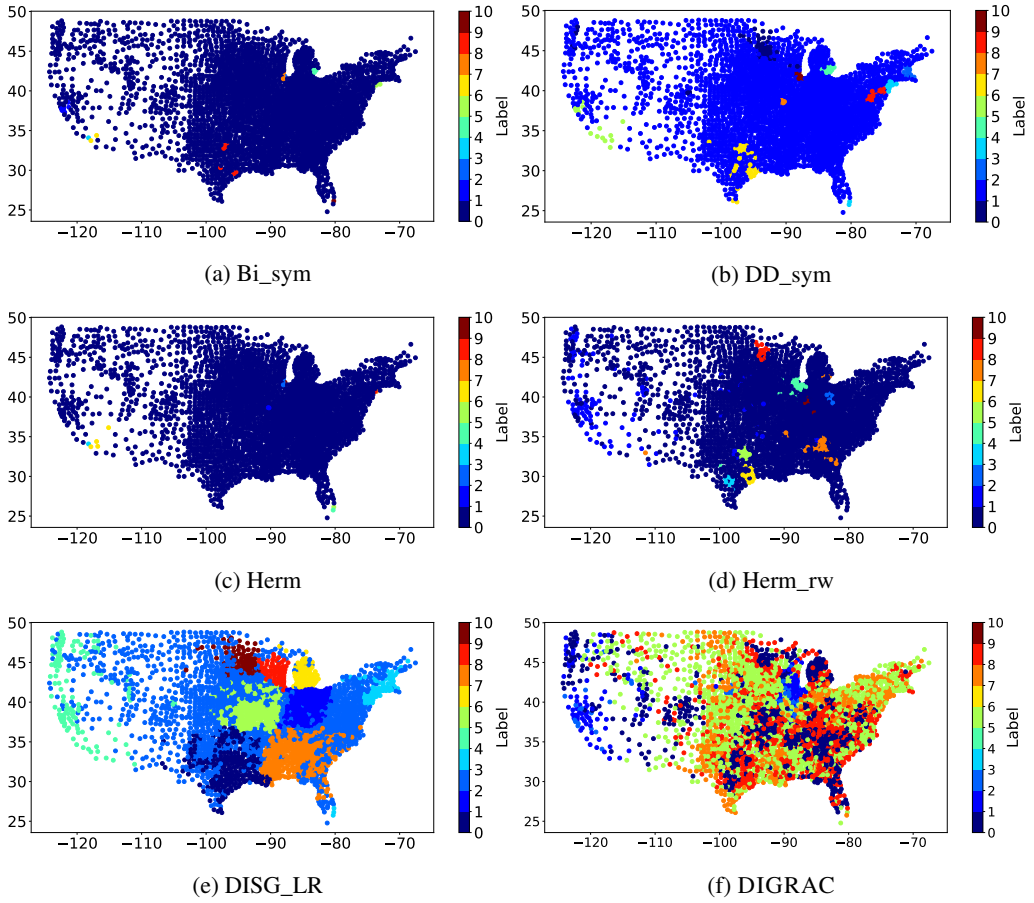

(a) Bi_sym (b) DD_sym

(c) Herm (d) Herm_rw

(e) DISG_LR (f) DIGRAC

Figure 17: US migration predicted clusters, along with the geographic locations of the counties.

D.5 Application to node classification and link direction prediction: details and additional results

Here we provide more details on the effect of LICE - adding our loss function $\mathcal{L}^{\text{sort}}_{\text{vol\_sum}}$ to the cross entropy loss in MagNet, DGCN, DiGCN, DiGCN_app, and DiGCN_ib. For a fair comparison of the methods, hyperparameters are not tuned; hence the methods may not achieve their optimal performance on the data sets. For *Cora-ML* and *CiteSeer* [4], we discover that their "ground-truth" labels do not give strong cut flow imbalance between classes, as shown in Figures 18b and 18d. Hence, as an imbalance-driven method, DIGRAC could not achieve leading performance in classification accuracy, as indicated in the first row of Table 10 and that of Table 11. Note that we train DIGRAC in a semi-supervised manner, applying cross-entropy loss and triplet loss on all training nodes, i.e., treating all training nodes as seed nodes. Details of the semi-supervised settings are discussed in appendix B.5. We use cross-entropy loss for all the comparing GNNs as the loss function.

As for link direction prediction, for each of the training, validation and test edges, the ratio of the two classes (forward and backward direction) is 1:1. We also provide the results for a more general link prediction task, a three-class classification problem (no link, forward and backward direction), assuming absence of bidirectional edges (such edges are rare in these two data sets, see Table 4). In this task, for each of the training, validation and test edges, the ratio of the three classes (no link, forward and backward direction) is 2:1:1. The result comparison table on the two methods mentioned in Table 2 of the main text, is given in Table 9, with similar conclusions as in the main text. Each of the methods applies cross-entropy loss to all training edges as a baseline variant. The comparing variant, ending with "+LI", uses LICE as the loss function, adding self-supervised imbalance loss $\mathcal{L}^{\text{sort}}_{\text{vol\_sum}}$ to the observed network (with all nodes in the network and all the training edges).

Table 9: Link prediction (three-class classification) test accuracy (%) on real data sets.

Data set	DGCN	DGCN+LI	Avg. gain (%)	DiGCN_app	DiGCN_app+LI	Avg. gain (%)
Cora-ML	68.58 ± 2.13	70.05 ± 0.78	1.47	62.27 ± 6.25	63.64 ± 4.54	1.37
CiteSeer	61.94 ± 3.87	63.32 ± 3.01	1.38	56.57 ± 1.55	56.86 ± 1.33	0.29

Node classification class probabilities are obtained via the same procedure as in the node clustering task. For each of both link prediction tasks, we concatenate the embeddings of each ordered node pair, then apply a linear layer followed by a unit *softmax* function to output the class probabilities from the first node to the second node in the ordered pair. For both tasks, we use 10 different data splits and average the results. Results are reported plus/minus one standard error.

Table 10: Performance comparison on *Cora-ML*. The best is marked in **bold red** and the second best is marked in underline blue.

Metric/Method	MagNet	DGCN	DiGCN	DiGCN_app	DiGCN_ib	DIGRAC
test accuracy(%)	64.29 ± 2.69	76.34 ± 6.03	37.55 ± 5.17	**78.31 ± 1.45**	74.59 ± 2.84	71.13 ± 4.80
test ARI	0.35±0.04	0.54±0.08	0.06±0.01	**0.56±0.03**	0.50±0.05	0.44±0.08
$\mathcal{O}^{\text{sort}}_{\text{vol\_sum}}$	0.03±0.01	0.01±0.00	**0.09±0.02**	0.01±0.00	0.01±0.00	0.03±0.01
$\mathcal{O}^{\text{sort}}_{\text{vol\_min}}$	0.21±0.03	0.27±0.06	**0.42±0.10**	0.20±0.04	0.22±0.05	0.40±0.07
$\mathcal{O}^{\text{sort}}_{\text{vol\_max}}$	0.02±0.01	0.01±0.00	**0.06±0.02**	0.01±0.00	0.01±0.00	0.02±0.01
$\mathcal{O}^{\text{sort}}_{\text{plain}}$	0.31±0.04	0.49±0.08	**0.82±0.10**	0.33±0.06	0.40±0.08	0.60±0.10
$\mathcal{O}^{\text{std}}_{\text{vol\_sum}}$	0.03±0.01	0.02±0.01	**0.09±0.03**	0.02±0.01	0.02±0.01	0.03±0.01
$\mathcal{O}^{\text{std}}_{\text{vol\_min}}$	0.27±0.03	0.26±0.10	**0.42±0.11**	0.29±0.12	0.27±0.04	0.41±0.08
$\mathcal{O}^{\text{std}}_{\text{vol\_max}}$	0.03±0.01	0.01±0.01	**0.07±0.02**	0.02±0.00	0.02±0.00	0.03±0.01
$\mathcal{O}^{\text{std}}_{\text{plain}}$	0.37±0.04	0.41±0.08	**0.77±0.10**	0.43±0.09	0.45±0.08	0.58±0.08
$\mathcal{O}^{\text{naive}}_{\text{vol\_sum}}$	0.02±0.00	0.01±0.00	**0.05±0.01**	0.01±0.00	0.01±0.00	0.02±0.00
$\mathcal{O}^{\text{naive}}_{\text{vol\_min}}$	0.14±0.02	0.18±0.04	**0.28±0.06**	0.13±0.02	0.15±0.03	0.26±0.05
$\mathcal{O}^{\text{naive}}_{\text{vol\_max}}$	0.01±0.00	0.01±0.00	**0.04±0.01**	0.01±0.00	0.01±0.00	0.01±0.00
$\mathcal{O}^{\text{naive}}_{\text{plain}}$	0.20±0.03	0.34±0.07	**0.60±0.07**	0.22±0.04	0.27±0.05	0.40±0.07
size ratio	3.00	33.90	27.04	3.62	3.84	**2.94**
size std	150.83	204.99	535.45	167.50	163.82	**132.88**

Table 11: Performance comparison on *CiteSeer*. The best is marked in **bold red** and the second best is marked in underline blue.

Metric/Method	MagNet	DGCN	DiGCN	DiGCN_app	DiGCN_ib	DIGRAC
test accuracy(%)	52.77 ± 7.11	50.93 ± 4.27	31.89 ± 3.87	**60.95 ± 1.97**	37.33 ± 9.14	54.68 ± 2.24
test ARI	0.23±0.07	0.23±0.04	0.04±0.01	**0.32±0.02**	0.10±0.05	0.24±0.03
$\mathcal{O}^{\text{sort}}_{\text{vol\_sum}}$	0.05±0.03	0.01±0.00	**0.09±0.02**	0.01±0.00	0.02±0.00	0.03±0.01
$\mathcal{O}^{\text{sort}}_{\text{vol\_min}}$	0.30±0.12	0.10±0.04	**0.34±0.09**	0.15±0.03	0.12±0.04	**0.34±0.09**
$\mathcal{O}^{\text{sort}}_{\text{vol\_max}}$	0.04±0.03	0.01±0.00	**0.06±0.02**	0.01±0.00	0.01±0.00	0.03±0.01
$\mathcal{O}^{\text{sort}}_{\text{plain}}$	0.43±0.15	0.42±0.11	**0.82±0.10**	0.27±0.05	0.45±0.13	0.55±0.13
$\mathcal{O}^{\text{std}}_{\text{vol\_sum}}$	0.06±0.02	0.02±0.01	**0.12±0.02**	0.02±0.01	0.03±0.01	0.04±0.01
$\mathcal{O}^{\text{std}}_{\text{vol\_min}}$	0.33±0.09	0.18±0.12	**0.43±0.09**	0.27±0.10	0.20±0.07	0.36±0.09
$\mathcal{O}^{\text{std}}_{\text{vol\_max}}$	0.05±0.02	0.01±0.01	**0.08±0.01**	0.02±0.01	0.02±0.01	0.03±0.01
$\mathcal{O}^{\text{std}}_{\text{plain}}$	0.48±0.08	0.38±0.12	**0.86±0.05**	0.39±0.10	0.42±0.07	0.58±0.08
$\mathcal{O}^{\text{naive}}_{\text{vol\_sum}}$	0.04±0.02	0.01±0.00	**0.07±0.01**	0.01±0.00	0.01±0.00	0.02±0.01
$\mathcal{O}^{\text{naive}}_{\text{vol\_min}}$	0.21±0.08	0.08±0.02	**0.27±0.05**	0.10±0.02	0.09±0.03	0.25±0.07
$\mathcal{O}^{\text{naive}}_{\text{vol\_max}}$	0.03±0.02	0.00±0.00	**0.05±0.01**	0.01±0.00	0.01±0.00	0.02±0.01
$\mathcal{O}^{\text{naive}}_{\text{plain}}$	0.31±0.11	0.33±0.09	**0.72±0.05**	0.19±0.04	0.33±0.09	0.40±0.10
size ratio	**2.01**	45.98	78.22	3.03	236.04	2.68
size std	**121.60**	396.29	615.75	175.07	495.90	160.99

Figure 18 displays the fitted flow matrices for both data sets. We can see that DIGRAC constructs clusters with higher cut flow imbalance than “ground-truth" labels. The ranked pairwise imbalance

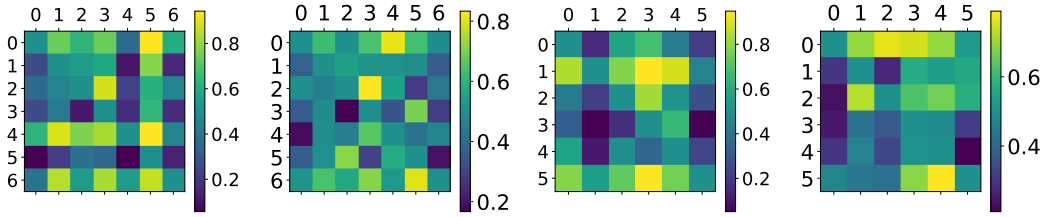

(a) *Cora-ML* by DIGRAC. (b) *Cora-ML* by labels. (c) *CiteSeer* by DIGRAC. (d) *CiteSeer* by labels.

Figure 18: Predicted meta-graph flow matrices from DIGRAC and “ground-truth" labels on *Cora-ML* and *CiteSeer*.

scores are shown in Figures 19 and 20, where DIGRAC attains an overall leading performance.

Tables 12 and 13 provide the results when GNNs are trained on LICE loss and DIGRAC is trained on only self-supervised loss but not cross-entropy loss. The NA entries for test accuracy of DIGRAC in Tables 12 and 13 arise because accuracy is not a permutation-invariant measure with respect to label indexing. Instead, we provide another row, test ARI, to compare the performance. Comparing Tables 10, 11, 12, and 13, we conclude that changing the loss from cross entropy to LICE on the few training nodes in a semi-supervised manner, there is a modest gain in imbalance scores in MagNet on both data sets, and in DiGCN on *CiteSeer*. We also observe slight test accuracy improvements for DiGCN and DiGCN_ib on *Cora-ML*, and for all GNNs except MagNet on *CiteSeer*, when replacing the cross-entropy loss with LICE. Note that the gain would be expected to be only marginal, since the imbalance loss is applied only to the induced subgraph of the training nodes (a small portion of all nodes). DIGRAC, on the other hand, achieves on average a larger amount of imbalance gain when switching the loss from semi-supervised to self-supervised. This also indicates the large influence of labels used during training.

Table 12: Performance comparison on *Cora-ML* when comparing GNNs use LICE as loss and DIGRAC uses only self-supervised imbalance loss. The best is marked in **bold red** and the second best is marked in underline blue.

Metric/Method	MagNet	DGCN	DiGCN	DiGCN_app	DiGCN_ib	DIGRAC
test accuracy(%)	62.50±2.17	75.35±3.89	38.89±5.20	**77.22±1.93**	75.14±2.89	NA
test ARI	0.32±0.03	**0.54±0.05**	0.06±0.02	**0.54±0.04**	0.51±0.05	0.02±0.01
$\mathcal{O}^{\text{sort}}_{\text{vol\_sum}}$	0.03±0.01	0.01±0.00	**0.09±0.02**	0.01±0.00	0.01±0.00	0.08±0.02
$\mathcal{O}^{\text{sort}}_{\text{vol\_min}}$	0.24±0.08	0.25±0.05	**0.41±0.10**	0.23±0.03	0.27±0.06	0.28±0.09
$\mathcal{O}^{\text{sort}}_{\text{vol\_max}}$	0.03±0.01	0.01±0.00	**0.07±0.02**	0.01±0.00	0.01±0.00	0.06±0.01
$\mathcal{O}^{\text{sort}}_{\text{plain}}$	0.36±0.10	0.45±0.11	0.83±0.06	0.34±0.04	0.43±0.09	**0.93±0.05**
$\mathcal{O}^{\text{std}}_{\text{vol\_sum}}$	0.04±0.01	0.02±0.01	**0.09±0.02**	0.02±0.00	0.02±0.01	0.08±0.01
$\mathcal{O}^{\text{std}}_{\text{vol\_min}}$	0.26±0.06	0.25±0.07	**0.40±0.10**	0.29±0.08	0.28±0.08	0.24±0.06
$\mathcal{O}^{\text{std}}_{\text{vol\_max}}$	0.03±0.01	0.02±0.01	**0.07±0.02**	0.02±0.00	0.02±0.01	0.06±0.01
$\mathcal{O}^{\text{std}}_{\text{plain}}$	0.38±0.06	0.39±0.09	0.77±0.06	0.41±0.09	0.48±0.10	**0.80±0.04**
$\mathcal{O}^{\text{naive}}_{\text{vol\_sum}}$	0.02±0.01	0.01±0.00	0.05±0.01	0.01±0.00	0.01±0.00	**0.06±0.01**
$\mathcal{O}^{\text{naive}}_{\text{vol\_min}}$	0.15±0.06	0.18±0.03	**0.26±0.06**	0.15±0.01	0.18±0.04	0.18±0.07
$\mathcal{O}^{\text{naive}}_{\text{vol\_max}}$	0.02±0.01	0.01±0.00	**0.04±0.01**	0.01±0.00	0.01±0.00	**0.04±0.01**
$\mathcal{O}^{\text{naive}}_{\text{plain}}$	0.23±0.07	0.32±0.08	0.58±0.05	0.23±0.03	0.28±0.06	**0.77±0.09**
size ratio	**3.14**	8.71	33.39	3.37	3.48	103.39
size std	154.48	196.24	516.89	**154.43**	164.40	435.63

For *Cora-ML* and *CiteSeer*, the ranked pairs imbalance scores for these loss functions are shown in Figures 21 and 22; DIGRAC again attains an overall satisfactory performance. Compared with Figures 19 and 20, when removing the supervised loss and only keeping the self-supervised imbalance loss, DIGRAC seems to perform better in terms of imbalance scores.

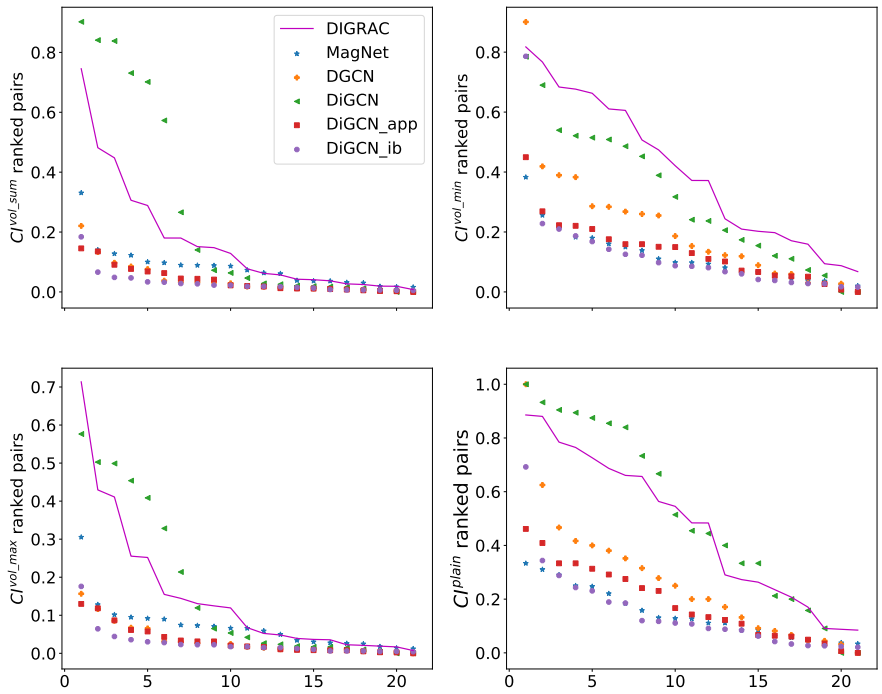

Figure 19: Ranked pairs of pairwise imbalance recovered by comparing methods for different choices of normalization on *Cora-ML* data set. Lines are used to highlight DIGRAC's performance.

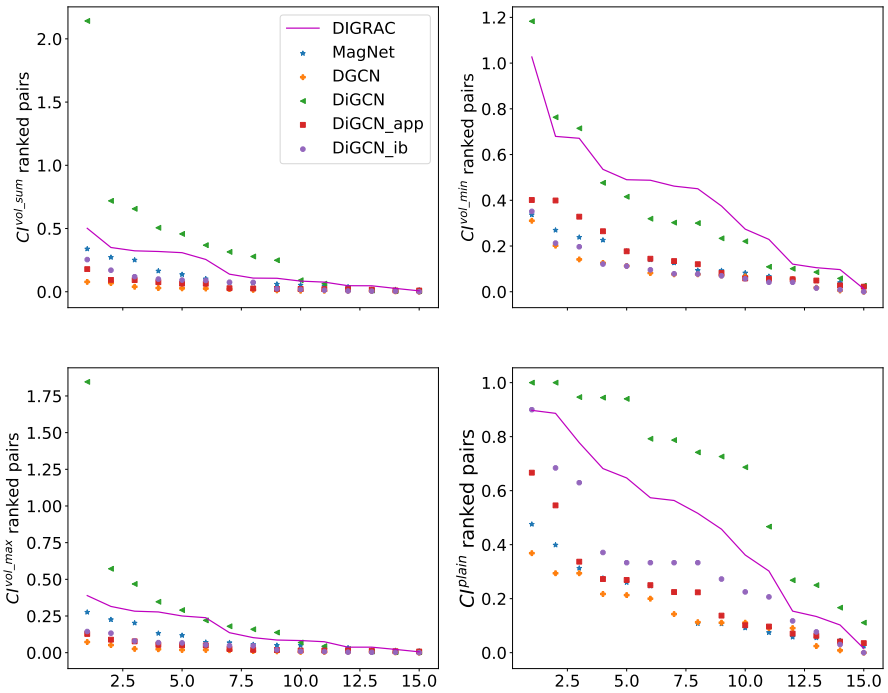

Figure 20: Ranked pairs of pairwise imbalance recovered by comparing methods for different choices of normalization on *CiteSeer* data set. Lines are used to highlight DIGRAC's performance.

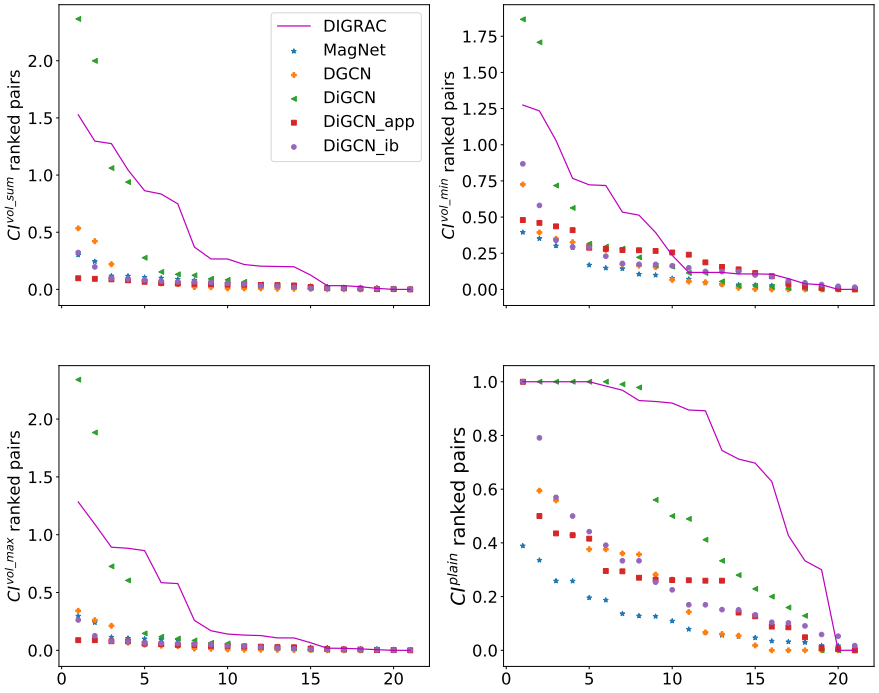

Figure 21: Ranked pairs of pairwise imbalance recovered by comparing methods for different choices of normalization on *Cora-ML* data set, where comparing GNNs use LICE as loss and DIGRAC only uses self-supervised imbalance loss. Lines are used to highlight DIGRAC's performance.

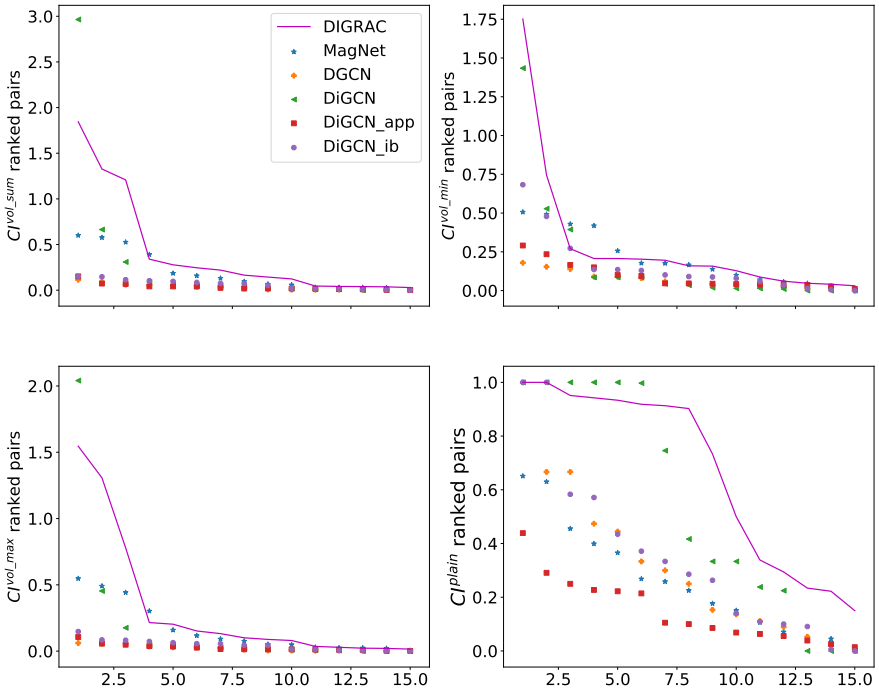

Figure 22: Ranked pairs of pairwise imbalance recovered by comparing methods for different choices of normalization on *CiteSeer* data set, where comparing GNNs use LICE as loss and DIGRAC only uses self-supervised imbalance loss. Lines are used to highlight DIGRAC's performance.

Table 13: Performance comparison on *CiteSeer* when comparing GNNs use LICE as loss and DIGRAC uses only self-supervised imbalance loss. The best is marked in **bold red** and the second best is marked in underline blue.

Metric/Method	MagNet	DGCN	DiGCN	DiGCN_app	DiGCN_ib	DIGRAC
test accuracy(%)	48.73±8.98	53.16±4.60	32.06±3.43	**61.72±1.50**	39.60±8.14	NA
test ARI	0.19±0.08	0.23±0.03	0.04±0.01	**0.32±0.02**	0.11±0.06	0.03±0.01
$\mathcal{O}^{\text{sort}}_{\text{vol\_sum}}$	0.07±0.03	0.01±0.00	0.10±0.03	0.01±0.00	0.01±0.00	**0.11±0.03**
$\mathcal{O}^{\text{sort}}_{\text{vol\_min}}$	0.33±0.12	0.12±0.04	0.32±0.12	0.14±0.03	0.11±0.05	**0.38±0.15**
$\mathcal{O}^{\text{sort}}_{\text{vol\_max}}$	0.06±0.03	0.01±0.00	0.08±0.03	0.01±0.00	0.01±0.00	**0.09±0.02**
$\mathcal{O}^{\text{sort}}_{\text{plain}}$	0.47±0.14	0.36±0.08	0.80±0.17	0.25±0.05	0.48±0.12	**0.89±0.09**
$\mathcal{O}^{\text{std}}_{\text{vol\_sum}}$	0.07±0.02	0.01±0.01	**0.14±0.04**	0.01±0.01	0.03±0.01	0.10±0.02
$\mathcal{O}^{\text{std}}_{\text{vol\_min}}$	0.34±0.08	0.13±0.09	**0.41±0.10**	0.20±0.10	0.20±0.09	0.35±0.12
$\mathcal{O}^{\text{std}}_{\text{vol\_max}}$	0.06±0.02	0.01±0.01	**0.10±0.03**	0.01±0.01	0.02±0.01	0.08±0.02
$\mathcal{O}^{\text{std}}_{\text{plain}}$	0.50±0.09	0.34±0.10	**0.89±0.07**	0.34±0.17	0.44±0.13	0.84±0.08
$\mathcal{O}^{\text{naive}}_{\text{vol\_sum}}$	0.05±0.02	0.01±0.00	**0.08±0.03**	0.01±0.00	0.01±0.00	**0.08±0.02**
$\mathcal{O}^{\text{naive}}_{\text{vol\_min}}$	0.23±0.09	0.10±0.04	0.25±0.09	0.10±0.02	0.08±0.03	**0.28±0.11**
$\mathcal{O}^{\text{naive}}_{\text{vol\_max}}$	0.04±0.02	0.00±0.00	**0.06±0.02**	0.01±0.00	0.01±0.00	**0.06±0.02**
$\mathcal{O}^{\text{naive}}_{\text{plain}}$	0.33±0.10	0.30±0.07	0.69±0.04	0.18±0.03	0.35±0.10	**0.73±0.07**
size ratio	**2.12**	184.72	48.29	2.84	79.12	222.24
size std	**129.43**	370.57	585.07	164.54	446.87	407.21